NANO · MICRO small
www.small-journal.com

Ultrafast Synthesis of Single-Atom Catalysts for Electrocatalytic Applications

Boran Zhou, Kaiyuan Liu, Kedi Yu, Qiang Zhou, Yan Gao, Xin Gao,* Zhengbo Chen,* Wenxing Chen,* and Pengwan Chen**

A recent development in catalytic research, single-atom catalysts (SACs) are one of the most significant categories of catalytic materials. During preparation, individual atoms migrate and agglomerate due to the high surface free energy. The rapid thermal shock strategy addresses this challenge by employing instantaneous high-temperature pulses to synthesize SACs, while minimizing heating duration to prevent metal aggregation and substrate degradation, thereby preserving atomic-level dispersion. The resultant SACs exhibit exceptional catalytic activity, remarkable selectivity, and long-term stability, which have attracted extensive attention in electrocatalysis. In this paper, cutting-edge ultrafast synthesis techniques such as Joule heating, microwave radiation, pulsed discharge, and arc discharge are comprehensively analyzed. Their ability is emphasized to achieve uniform dispersion of separated metal atoms and optimize the catalytic activity for electrocatalytic applications. A systematic summary of SACs synthesized by these rapid methods is provided, with particular emphasis on their implementation in carbon dioxide reduction reaction (CO_2RR), oxygen evolution reaction (OER), hydrogen evolution reaction (HER), and oxygen reduction reaction (ORR) systems. The review provides an in-depth discussion on the rapid synthesis strategy for development trend, remaining challenges, and the application prospects in electrocatalysis.

1. Introduction

Electrocatalysts are pivotal in various high-performance energy devices and are integral to these electrochemical reactions.[1–6] It is still difficult to develop electrocatalysts and improve their electrochemical performance. Heterogeneous catalysts typically possess active sites characterized by metal centers. Metal particle size reduction is an efficient way to improve catalytic activity. The surface atomic structure, electrical structure, and surface flaws are all changed by the large increase in exposed surface atoms.[7,8] With their many highly active surface sites, and superior geometric and electrical effects, these materials show great prospects for catalytic applications.[9,10]

The active site of isolated metal atoms of single-atom catalysts (SACs) is anchored by the coordination sites of the surrounding solid supports. Its electronic architecture and energy level orbital differ from those of metallic nanoparticles, which can maximize metal dispersion and atomic utilization efficiency.[11] Clusters aggregate as the rising surface free energy of metal atoms. A feasible method to prevent this aggregation is to use appropriate carrier materials that strongly interact with the metal atoms.[12–15] Currently, several synthesis techniques are being investigated to create a consistent dispersion of metal atoms in SACs. For instance, methods such as impregnation,[16] co-precipitation,[17] and atomic layer deposition (ALD)[18,19] are employed. However, the preparation process of ALD, which

B. Zhou, K. Liu, P. Chen
School of Materials Science and Engineering
Beijing Institute of Technology
Beijing 100081, P. R. China
E-mail: pwchen@bit.edu.cn

B. Zhou, K. Yu, Z. Chen
Department of Chemistry
Capital Normal University
Beijing 100048, P. R. China
E-mail: czb979216@sina.com

Q. Zhou
China Academy of Ordnance Science
Beijing 100089, P. R. China

Y. Gao
AnHui Provincial Engineering Research Center of Silicon-Based Materials
Bengbu University
Bengbu, Anhui 233030, P. R. China
E-mail: gaoyan@bbc.edu.cn

X. Gao
School of Mechatronical Engineering
Beijing Institute of Technology
Beijing 100081, P. R. China
E-mail: gaoxin@bit.edu.cn

W. Chen
Energy & Catalysis Center
School of Materials Science and Engineering
Beijing Institute of Technology
Beijing 100081, P. R. China
E-mail: wxchen@bit.edu.cn

P. Chen
Yangtze Delta Region Academy of Beijing Institute of Technology
Jiaxing, Zhejiang 314019, P. R. China

The ORCID identification number(s) for the author(s) of this article can be found under https://doi.org/10.1002/smll.202501917

DOI: 10.1002/smll.202501917

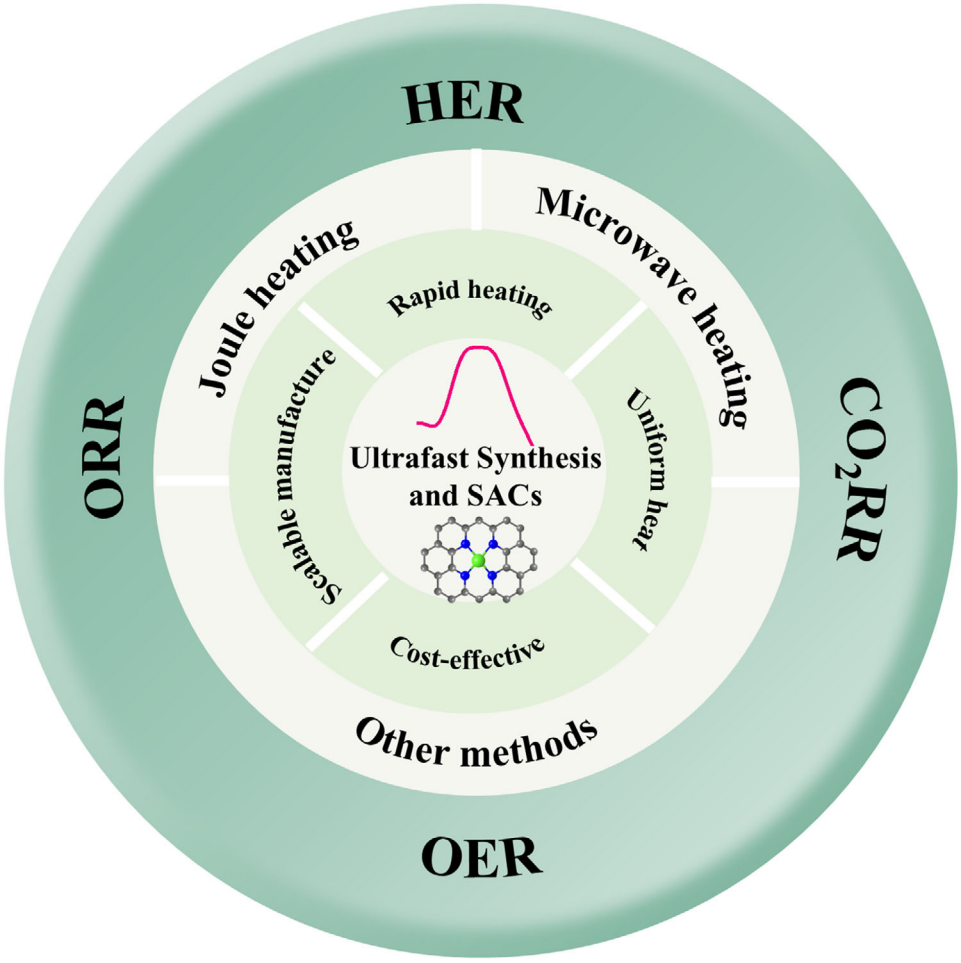

Figure 1. The classified diagram of the primary strategies of ultrafast synthetic SACs.

requires high vacuum conditions, is complex, and the method suffers from low yield and expensive equipment, making large-scale production difficult.[18,19] Impregnation and co-precipitation methods are limited by the limited types of prepared materials, complex preparation steps, and long processing time.[16,17] These shortcomings hinder further development and application. Therefore, it is essential to explore the rapid and simple synthetic strategies with industrial prospects.[20–26]

The ultrafast synthesis strategy is characterized by rapid ignition, rapid heating, and instantaneous quenching, while keeping the heating time very short to avoid the aggregation of metal atoms and the destruction of the support, thus maintaining single-atom dispersion.[12,27,28] At the same time, it can instantaneously produce ultra-high temperatures, which are essential for single-atom stability, as it provides sufficient activation energy to promote the formation of bonds between the single-atom and the substrate, resulting in excellent chemical stability during catalysis. As shown in **Figure 1**, several rapid thermal shock strategies have been developed to synthesize SACs, such as Joule heating,[27,29–33] microwave heating,[34–42] and pulsed discharge,[43] electric pulse method, arc discharge method, etc. The rapid thermal shock process has the following advantages: a) Rapid heating and quenching process, which prevents atomic diffusion and agglomeration; b) Heat is distributed uniformly throughout the material; c) The manufacturing process is controllable and the materials used to manufacture are scalable. These features have led to rapid thermal shock methods that allow for rapid and easy preparation of SACs, which has made tremendous progress in recent years (**Figure 2**).

At present, the application of SACs in the field of electrocatalysis is relatively innovative and has attracted extensive attention. The metal atoms in SACs are highly dispersed, which possess high catalytic activity and excellent selectivity during the catalytic process. Individual atom and support interactions can improve electrocatalytic performance. The rapid thermal shock method can be used to synthesize SACs for electrochemical applications.[44–53] As a unique catalyst, SACs have wide applications in electrocatalysis, such as carbon dioxide reduction reaction (CO_2RR),[54,55] oxygen evolution reaction (OER),[56–58] hydrogen evolution reaction (HER),[59,60] and oxygen reduction reaction (ORR),[61,62] etc. In this paper, various rapid synthesis methods for the preparation of SACs are reviewed. The effects of SACs on the atomic dispersion, catalytic activity and stability were summarized. Finally, we analyzed the electrocatalysis application of the above method. Finally, this paper discusses the future trends and challenges in the rapid preparation technologies of SACs.

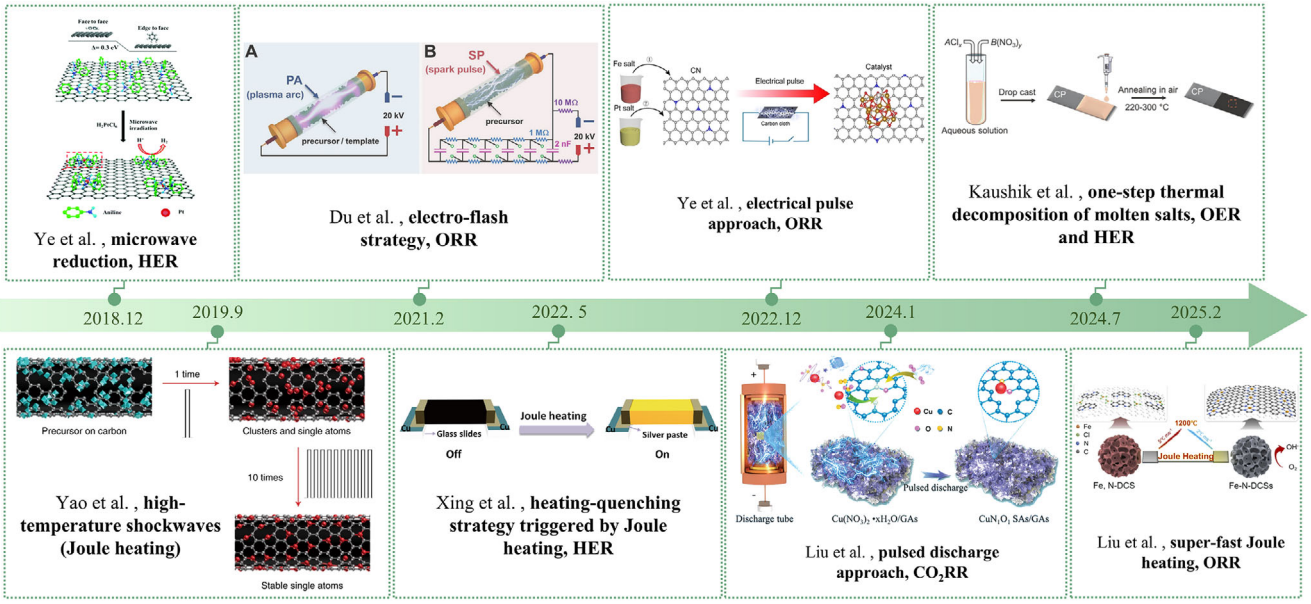

Figure 2. The development process of rapid heating approaches for synthetic SACs. Reproduced with permission.[27] Copyright 2019, Springer Nature. Reproduced with permission.[37] Copyright 2019, Royal Society of Chemistry. Reproduced with permission.[43] Copyright 2024, John Wiley and Sons. Reproduced with permission.[44] Copyright 2022, John Wiley and Sons. Reproduced with permission.[67] Copyright 2021, Springer Nature. Reproduced with permission.[68] Copyright 2025, Elsevier. Reproduced with permission.[88] Copyright 2021, John Wiley and Sons. Reproduced with permission.[91] Copyright 2024, John Wiley and Sons.

2. Ultrafast Synthetic Strategies

2.1. Joule Heating

Joule heating can quickly convert electrical energy into thermal energy and is an efficient and well-controlled method for materials synthesis. Joule heating strategies are characterized by high maximum temperatures, ultra-fast heating and quenching. Joule heating can quickly reach temperatures of up to 3000 K, effectively overcoming the limitations imposed by traditional heating methods.[46] In addition to preventing Ostwald ripening and nanoparticle aggregation, flash quenching can produce new phase structures. In recent years, Joule heating has been a popular method for creating catalytic materials, such as nanoparticles,[63,64] high-entropy alloy nanomaterials,[65,66] and single-atomic materials.[13,30,31,33,67,68]

Xing et al.[67] developed a transient heating-quenching method for the synthesis of nitrogen-doped graphene-supported single-atom cobalt materials (CoNG-JH) with a 3D porous monolithic structure by Joule heating (**Figure 3a**). As shown in Figure 3b, CoNG-JH has abundant mesopores. The pore size distribution curves showed that CoNG-JH contained micropores, mesopores and macropores. The I_D/I_G of CoNG-JH and CoG-JH is higher than that of precursors (Figure 3c). According to this, Joule heating encourages the creation of defect sites that single atoms can exploit as anchoring sites. Combined with the characterization results, CoNG-JH synthesized by Joule heating technology has atomically dispersed CoN_x. The method can incorporate metal atoms and nitrogen atoms to the graphene, and reduce graphene oxide in less than two seconds. By avoiding prolonged heating to cause atomic aggregation, the atomic-scale CoN_x active sites are rapidly and stably dispersed in graphene under instantaneous quenching conditions. Lin et al.[69] used rapid Joule heating to prepare Ru single atoms embedded into the subsurface lattice of Ni_3FeN (Ni_3FeN-Ru_{buried}) in a two-step method (Figure 3d): 1) Introducing Ru atoms into NiFe chloride oxide as a precursor; 2) Rapid Joule heating synthesis was used to nitride the obtained precursor into a buried layer of anti-perovskite Ni_3FeN-Ruburied with buried Ru atoms. In addition, surface-loaded individual Ru atoms (Ni_3FeN-$Ru_{surface}$) are annealed for long periods in a tube furnace by conventional nitriding strategies (Figure 3d). The unique structure of the material is held and frozen by rapid Joule heating synthesis, which combines rapid heating and quenching operations. This enables the focused design and manufacture of electrocatalysts with a customized coordinating environment.

Liu et al.[68] reported a technique to bind Fe single atoms to freshly made defective porous carbon spheres (Fe-N-DCSs) through ultrafast Joule heating in milliseconds. A schematic diagram of Fe-N-DCSs is shown in Figure 3e. The nitrogen element was doped into the produced defective porous carbon spheres[70] utilizing 1,10-benzotriazole as a source of nitrogen. Then, Fe^{3+} ions are adsorbed into N-doped carbon spheres through impregnation forming precursors. Then, Fe-N-DCSs were prepared through the Joule heating method. The scanning electron microscope (SEM) image revealed spherical topography with an average diameter of about 100 nm (Figure 3f). In Figure 3g, it shows that the position of the absorption edge of Fe-N-DCSs is similar to that of FePc. And it indicates that it is in the vicinity of the 2^+ oxidation state. This method can effectively avoid SACs with high free energy from clumping together during long-term pyrolysis at high temperature. It also avoids the loss of profitable N specials.[71–73]

Qin et al.[74] prepared highly efficient synthesized and actively modulated catalysts using flash joule heating technology

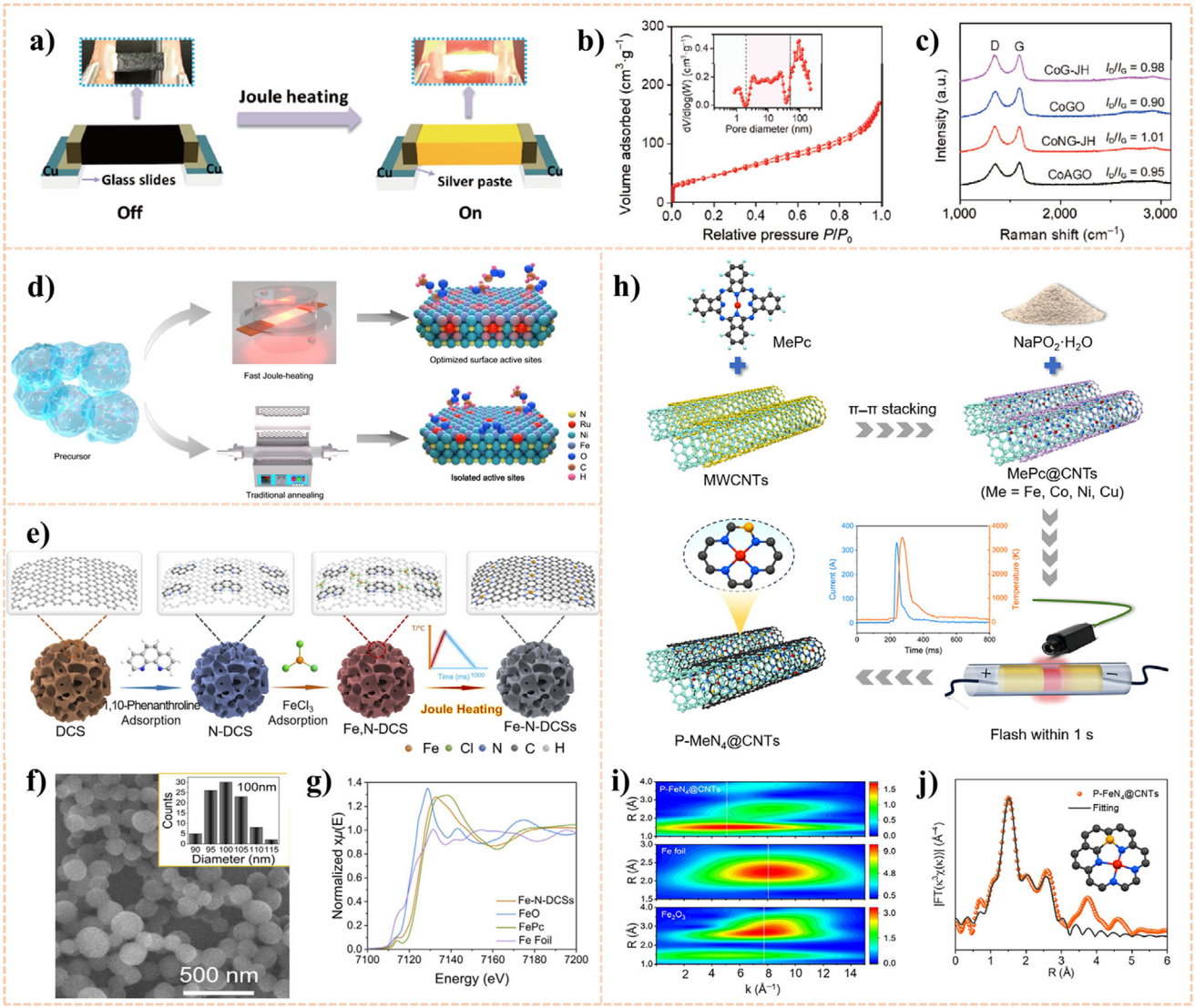

Figure 3. a) Diagram of the CoAGO aerogel films by electrical Joule heating process: heating and quenching were accomplished instantly with on/off status. b) Curves of CoNG-JH nitrogen adsorption and desorption. It displays the curve of CoNG-JH pore-size distribution in the inset. c) Raman spectra of CoAGO, CoGO, CoNG-JH, and CoG-JH. Reproduced with permission.[67] Copyright 2021, Springer Nature. d) Illustration of the synthesis strategy of $Ni_3FeN\text{-}Ru_{buried}$. Reproduced with permission.[69] Copyright 2025, Springer Nature. e) Schematic illustration of the preparation for Fe-N-DCSs. f) SEM image of Fe-N-DCSs. g) Normalized XANES spectra of Fe-N-DCSs, FeO, FePc, and Fe Foil at the Fe K-edge. Reproduced with permission.[68] Copyright 2025, Elsevier. h) Schematic diagram showing the synthesis process of atomically-dispersed catalysts of P-MeN_4@CNTs (Me = Fe, Co, Ni, and Cu). i) k^3-weighted wavelet-transformed Fe K edge EXAFS spectra of P-FeN_4@CNTs, Fe_2O_3, and Fe foil. j) EXAFS fitting curve and atomic configuration of P-FeN_4@CNTs. Reproduced with permission.[74] Copyright 2024, Elsevier.

(Figure 3h). The wavelet-transformed (WT) extended X-ray absorption fine structure (EXAFS) plots were used to study the coordination environment (Figure 3i). In contrast to the properties of Fe foil and Fe_2O_3, the WT plot of P-FeN_4@CNT shows maximum intensity at 5.2 $Å^{-1}$. Least squares EXAFS fitting was used to examine the partial geometry of Fe in P-FeN_4@CNTs (Figure 3j). Fe atoms are uniformly dispersed in P-FeN_4@CNTs. And it coordinated with pyridine-N atoms to form the FeN_4 active site. In addition, the presence of P atoms binds to the adjacent N atoms to regulate the local structure. Atomically dispersive MeN_x sites are formed on the surface of carbon nanotube by the high heating rates and cooling rates (over 10^4 K s^{-1}) and instantaneous high temperatures (about 3535 K). This ultra-fast thermal shock technology can manipulate components or incorporate heteroatoms to increase catalytic activity while preventing the aggregation of isolated metal atoms.

Joule heating uses heat on a conductive substrate to create nanomaterials in situ at a very quick rate of response. In addition to providing exceptionally high temperatures to create robust contacts between metal atoms and substrates, the quick heating and cooling rates of Joule heating might restrict phase separation or atomic diffusion and agglomeration during synthesis. The joule heating technique turns on/off the Joule heating shockwave repeatedly, transforming the nanoparticles into individually

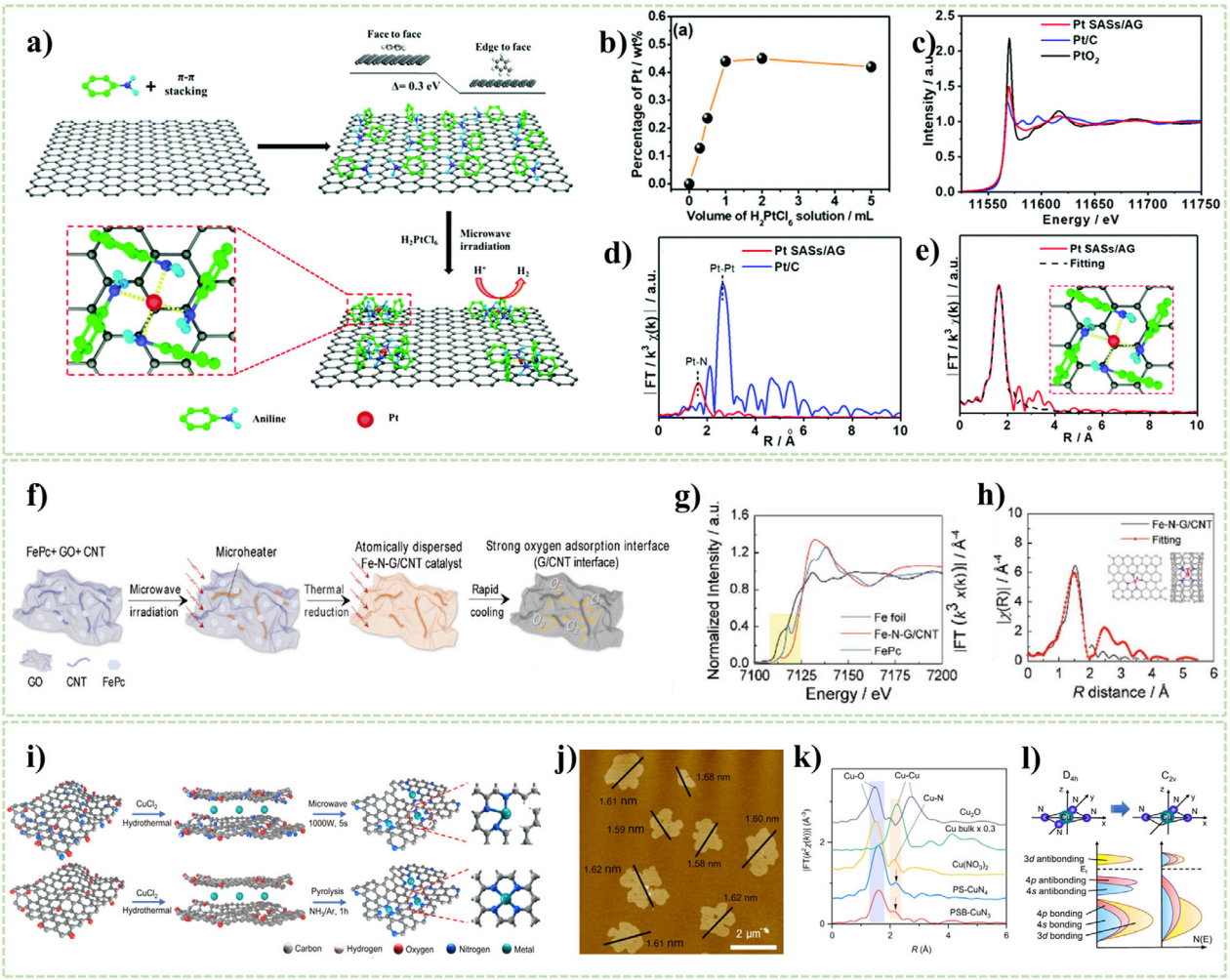

Figure 4. a) Synthetic illustration of Pt SASs/AG. b) Mass percentages of Pt in Pt SASs/AG samples made with different volumes of H_2PtCl_6 solution. c) XANES spectra of Pt SASs/AG, Pt/C, and Pt foil. d) FT-EXAFS spectra of the Pt L_3-edge of Pt SASs/AG and Pt/C. e) EXAFS R-space fitting curve of the Pt SASs/AG. Reproduced with permission.[37] Copyright 2019, Royal Society of Chemistry. f) Schematic of the preparation of Fe-N-G/CNT. g) Fe K-edge XANES spectra of Fe-N-G/CNT, Fe foil, and FePc. h) EXAFS fitting curve of Fe-N-G/CNT R-space. Reproduced with permission.[38] Copyright 2021, John Wiley and Sons. i) Illustration of Synthetic method for PSB-CuN_3 and PS-CuN_4. j) AFM image of prepared PSB-CuN_3. k) Fourier-transformed magnitudes of the Cu K-edge EXAFS signals. l) Schematic illustration of band shifts and hybridization. Reproduced with permission.[39] Copyright 2023, Springer Nature.

distributed atoms that are stable. It can be seen from the above application examples that the maneuverability of the Joule heating method can help to maintain the unique atomic dispersive feature of the prepared material and improve the catalytic activity of the catalyst. Therefore, Joule heating will make it possible to enable controlled and scalable production of SACs.

2.2. Microwave Heating

Microwave heating has been widely used in recent years.[75–79] Among them, the sample directly absorbs microwaves which are efficiently converted into heat energy. The microwave heating method can prepare SACs in a short time.[77,80,81]

The synthesis of SACs has made extensive use of reduced graphene oxide (rGO), which also serves as a microwave absorber.[34,37,42,82,83] Ye et al.[37] developed a simple aniline-anchored-microwave reduction approach to prepare a Pt single atom (Pt SASs/AG) anchored to aniline-stacked graphene (**Figure 4**a). Figure 4b shows the amount of load on the Pt atom. The content of Pt increased with the increase of the volume of H_2PtCl_6. The content of Pt remained almost stable after more than 1 mL. Figure 4c shows that the dense WL of Pt SASs/AG indicates an increase in vacancies in the Pt d orbital.[84,85] The absence of Pt-Pt coordination peaks suggests that the Pt sites are dispersive on graphene (Figure 4d). According to the fitting curve (Figure 4e), the Pt-N configuration is formed by Pt single atoms coordinating with four aniline molecules, as seen in the inset Figure 4e. This work has two advantages: a) Excess Pt cannot be anchored at maximum aniline protonation. Pt clusters and nanoparticles will not form because of this. b) Pt SAS cannot sinter since microwave reduction does not require harsh

circumstances like high temperatures. Meng et al.[38] developed a one-step microwave-assisted approach for creating a single-atom iron with coordinating nitrogen on a graphene/CNT hybrid electrocatalyst (Fe-N-G/CNT), as shown in Figure 4f. Compared to the Fe foil and FePc reference materials, the X-ray absorption near edge structure (XANES) spectra of the Fe-N-G/CNT have moved to a higher energy (Figure 4g). The EXAFS fitting curve is displayed in Figure 4h. This suggests that the isolated Fe atoms are positively charged. The main peak at 1.56 nm exhibited Fe-N coordination, suggesting that nitrogen (Fe-N) stabilized the solitary Fe atom. With this knowledge, the Fe-N_4 coordination structure serves as the primary anchor for the Fe atom on graphene and carbon nanotubes (Figure 4h inset). The study by Meng et al.[38] develops a reasonable approach for the preparation of SACs under low oxygen concentrations and low temperature environments.

Dong et al.[39] synthesized a planarly symmetrically broken CuN_3 single atom (PSB-CuN_3) by microwave heating. PSB-CuN_3 was synthesized by a microwave heating strategy, as shown in Figure 4i. Cu^{2+} ions are immobilized by electrostatic interactions with amine-functionalized graphene nanosheets (AGNs). Then, PSB-CuN_3 is produced in five seconds using a quick microwave heating procedure. The average thickness of PSB-CuN_3 is ≈1.61 Å, as determined by atomic force microscopy (AFM) calculations (Figure 4j). EXAFS and XANES investigated the PSB-CuN_3 chemical state and coordination environment. Figure 4k displays the PSB-CuN_3 Cu K-edge FT-EXAFS data together with references. Similar to the prototype spectrum of the pyridine-N-based MN_4C_4 motif, PSB-CuN_3, and PS-CuN_4 both show a major peak at ≈1.60 nm and a subsatellite peak at ≈2.20 Å.[86] According to a thorough examination of the density of states (Figure 4l), the antibonding 4s and 4p states can be driven much higher beyond the Fermi energy by a loss in local symmetry from $D_{4\ h}$ in CuN_4C_4 to C_{2v} in CuN_3C_3. Compared with the thermal annealing method, microwave-induced instantaneous heating causes significant changes in the local environment in the material, thereby promoting the formation of local symmetry-breaking structures.

Microwave heating technology has the advantages of mild preparation conditions, microwave-induced instantaneous heating is conducive to the formation of special atomic coordination structures, and prepare various SACs. In order to achieve effective microwave heating, three main requirements should be met: a) a large number of surface functional groups ensure that there is enough frictional heat generated by rotation in an oscillating electric field; b) sufficient conductivity to produce eddy currents; and c) high thermal conductivity, which permits heat to diffuse swiftly and uniformly throughout the sample. When compared to traditional heating techniques, microwave heating methods offer the advantages: a) ultrafast heating and quenching rate, b) adjustable temperature of heating, c) homogeneous heating across supports, d) suitable for carbon supports of various sizes, e) simple equipment.

2.3. Other Methods

Recently, some researchers have begun to develop new heating strategies to rapidly prepare SACs. At present, the ultrafast synthesis methods have been extended to pulsed discharge, electric pulse, electric spark, laser implantation, etc.

Among them, the pulsed discharge method was applied to the preparation of SACs for the first time in 2024. Liu et al.[43] successfully prepared a graphene aerogel-anchored copper single-atom catalyst using a high-density current pulse for hundreds of microseconds (**Figure 5a**). Figure 5b shows an SEM image of CuN_1O_1 SAs/GAs, presenting a 3D porous graphene aerogel. In Figure 5c, the 3D color distribution of CuN_1O_1 SAs/GAs is displayed. The green bumps represent rGO, while the red bumps represent Cu atoms. Between the two Cu atoms, the average distance is ≈0.56 nm. The C K-edge of CuN_1O_1 SAs/GAs shows a minor peak at 288.8 eV in Figure 5d. Compared to the original GO, the peak value of CuN_1O_1 SAs/GAs is low. Figure 5e shows the asymmetric coordination portion of the proposed CuN_1O_1 SAs/GAs. Transient current pulses cause a shock effect that preserves the asymmetric and unsaturated Cu-N_1O_1 coordination structure. The pulsed discharge method is characterized by the generation of a strong electromagnetic field with a pulse current period of 10^2–10^3 μs and a peak of 10^5 A.[87] Thus, the pulsed power can completely sublimate the precursor under the right conditions to form a mixture of isolated individual atoms and ions. SACs are formed following quick cooling. It is possible to create some monoatomic materials with particular structures on support materials by carefully controlling the energy input and using the proper support materials.

Ye et al.[44] developed an electrically pulsed method for synthesizing atomically dispersed Pt in different oxide clusters using nitrogen-doped carbon (Pt_1-MO_x/CN) as a carrier (Figure 5f). Fe/CN, Pt/CN, and Pt_1-FeO_x/CN have the small particle size. Microporous carbon is created because the pore size of Pt_1-FeO_x/CN is comparable to that of CN (Figure 5g). The particles in Figure 5h do not exhibit any diffraction peaks. In Figure 5i, the Pt-O scattering peak moves to the lower R-value and decreases intensity when Pt_1-FeO_x/CN is compared to Pt_1-Fe_2O_3/CN. This suggests that the Pt-O distance in Pt_1-FeO_x/CN gets shorter and the Pt-O coordination number drops. In this study, ZIF-8-derived CN facilitates electron transport during electrical impulses and offers a high specific surface area for effective metal species dispersion and stability.

Zheng et al.[45] created metastable nanomaterials by developing a hydrogen-substituted graphitic diyne-assisted ultrafast spark synthesis (GAUSS) method (Figure 5j). The GAUSS platform can achieve a rate of over 10^5 K s^{-1} and temperature of 3286 K during 8 ms. The single-atom Co site is evenly distributed over the hydrogen-substituted graphdiyne aerogel (HGDY) support, according to high-Angle annular dark field scanning transmission electron microscopy (HAADF-STEM) pictures. Wavelet analysis indicates that a single-atom site was effectively synthesized on the HGDY (Figure 5k). While avoiding phase separation, coarsening, and maturation, high temperatures and rapid heating rates enable for synthesis of SACs. With the flexibility to regulate temperature, composition, reaction time, and environment, the GAUSS platform offers an effective method for creating a variety of metastable nanomaterials.

Du et al.[88] developed continuous high pressure (PA approach) and intermittent high pressure (SP approach) to create carbon-supported atomically dispersed metal catalysts (ADMCs) for carbonizing MOF precursors quickly using an electro-flash technique (**Figure 6a**). Atomically dispersed Co can be easily obtained on nitrogen-doped carbon with a controlled morphology

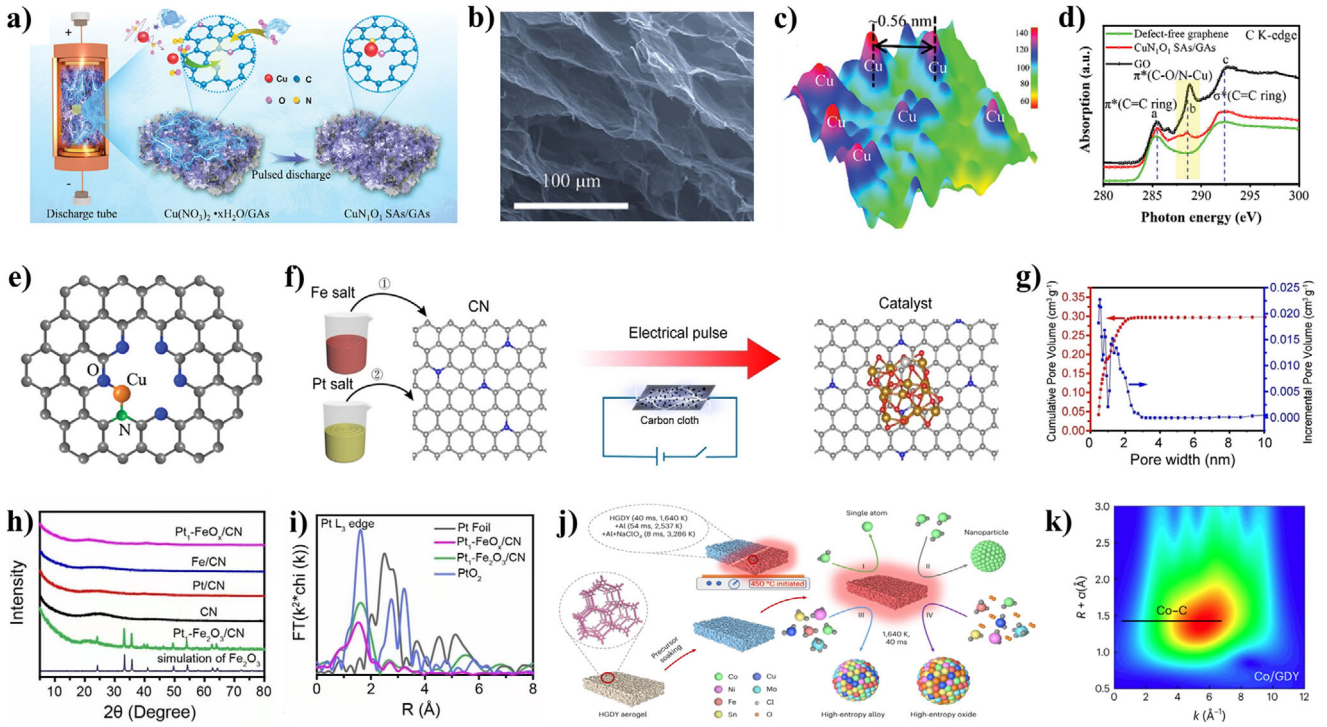

Figure 5. a) Schematic illustration of pulsed discharge method. b) SEM images of CuN_1O_1 SAs/GAs. c) The intensity distribution of CuN_1O_1 SAs/GAs. d) The C K-edge XANES spectra of CuN_1O_1 SAs/GAs, GO, and no defects graphene. e) Schematic diagram of CuN_1O_1 SAs/GAs atomic structure. Reproduced with permission.[43] Copyright 2024, John Wiley and Sons. f) Schematic diagram of the preparation of Pt_1-FeO_x/CN. g) Pore size distribution of Pt_1-FeO_x/CN. h) XRD patterns. i) R-space EXAFS of Pt L_3 edge of Pt_1-FeO_x/CN, Pt_1-Fe_2O_3/CN, Pt Foil, and PtO_2. Reproduced with permission.[44] Copyright 2022, John Wiley and Sons. j) Schematic of hydrogen-substituted GAUSS for metastable nanomaterials. k) Wavelet transforms for Co-HGDY. Reproduced with permission.[45] Copyright 2022, Springer Nature.

(2D nanosheets and 3D hollow nanospheres). Nitrogen-doped carbon nanosheets are produced by successive plasma arcs, and carbon hollow nanospheres are created by sporadic spark pulses using a blasting effect. Atomically distributed cobalt is used to embellish both structures. It is possible to obtain and preserve the faulty nature of the carbon support by limiting the processing duration of SP (Figure 6b). According to Figure 6c, the Co K-edge absorption peak of Co/N-C(SP) was in the middle of that of Co foil and Co_3O_4. In the above method, preventing their mobility and metallization at high voltages, metal ions are trapped in the MOF structure as nodes. Importantly, the electro-flash approach is appropriate for the commercial synthesis of carbon-backed ADMCs since gram-scale catalysts can be readily collected in less than an hour.

In addition to the above studies, Wang et al.[89] reported a one-step laser implant strategy (Figure 6d). The energy dispersive spectrometer (EDS) image show that the Pt, Ir, Cu, Co, and Ni atoms are evenly distributed on support (Figure 6e). The precursors are broken down into monolithic metal SAs by the laser pulses, which also enable the simultaneous creation of defects on the support. These SAs are anchored on the resulting defects through electrical interactions. With the laser injection method, SAs achieve the higher defect density and high load of 41.8 wt.%. Numerous metallic species have been successfully reduced to single atoms, nanoparticles, and nanoclusters, showing the resilience of strategy and wide range of applications. Xia et al.[90] developed a simple one-step ultra-high temperature arc discharge method to synthesize highly dispersed Pt single atoms, nanoclusters (NCs) and nanoparticles (NPs) with high-efficiency single-crystal MoC-supported platinum catalysts (Figure 6f). The charge differential density diagram was obtained by DFT calculation. Figure 6g shows that the electrons are redistributed on the prepared catalyst and transferred from MoC to Pt atoms. The high-temperature process also provides sufficient energy for the formation of Pt-MoC interactions, regulating adsorption performance and chemical transformation of small molecules. Kaushik et al.[91] reported a method for producing single atoms of noble metals loaded on non-noble metal oxides by one-step thermal breakdown of molten salts (Figure 6h). Noble metal single atoms are introduced into the non-noble metal oxide lattice through cation exchange in molten salts formed in situ and thermal decomposition of nitrate ions during heating. In Figure 6i, the intensity of Ir_1-Co_3O_4 is higher than that of Ir foil, indicating that there are more empty orbital states. It may be beneficial for improving the electrocatalytic activity. Figure 6j shows that Ir_1-Co_3O_4 has a main peak at 1.60 Å, which is similar to the peak of IrO_2, and Ir foil has a peak at 2.71 Å. The direct synthesis route is straightforward, minimizing uncontrollable variables often encountered in traditional multi-step processes, thus significantly reducing preparation time.

Kuai et al.[92] developed a micro-gas blasting (MGB) technique for producing metal oxide nanosheets (Pt_1/CeO_2-S) with a thickness of 3–8 nm and a high density of noble metal single-atom

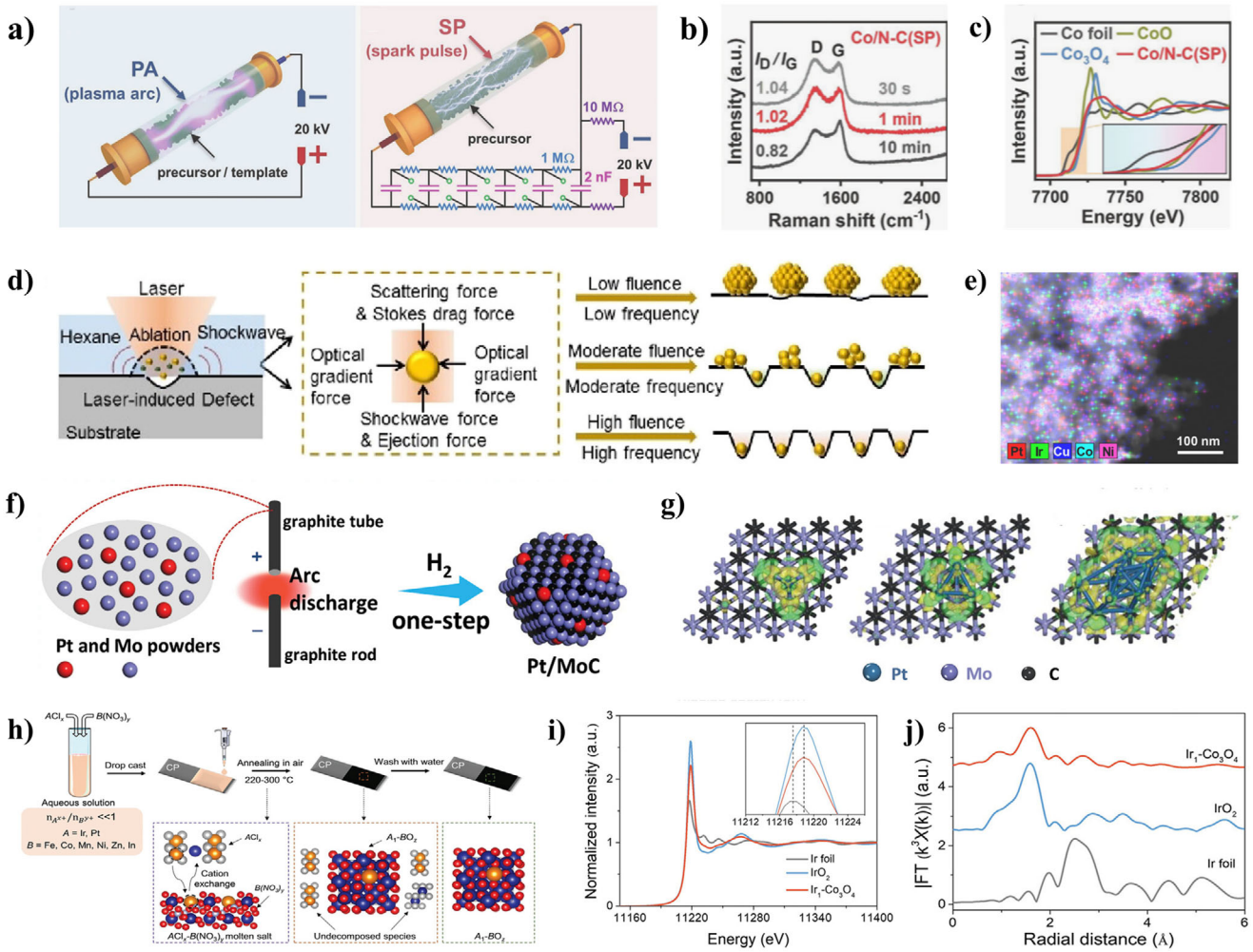

Figure 6. a) Schematic illustration of PA method and SP method. b) Raman spectra of Co/N-C(SP) exposed to a spark pulse for 30 s, 1 min and 10 min. c) Co K-edge EXAFS spectra for Co/N-C(SP), Co foil, CoO and Co_3O_4. Reproduced with permission.[88] Copyright 2021, John Wiely and Sons. d) Schematic depiction of the synthesis of Pt SAs under laser implantation. e) STEM and EDS mapping of CB-supported HESAs. Reproduced with permission.[89] Copyright 2023, American Chemical Society. f) Schematic illustration of synthesizing Pt/MoC catalysts via arc discharge procedure. g) Schematic diagram of the atomic structure of Pt/MoC. Reproduced with permission.[90] Copyright 2024, John Wiley and Sons. h) Schematic representation of the synthetic route of SACs. CP denotes carbon paper. i) Ir-L_3 edge XANES spectra of Ir_1-Co_3O_4, Irfoil, and IrO_2. j) Ir-L_3 edge EXAFS spectra of Ir1-Co_3O_4 and references. k) HAADF-STEM images of Ir1-Co3O4. Reproduced with permission.[91] Copyright 2024, John Wiley and Sons.

(**Figure** 7a). The AFM image confirms the presence of nanosheet structures (Figure 7b,c). The synthesis of MGB is a type of chemical reaction that is limited by space. It was easily scaled to obtain a multifunctional metal-oxide nanosheet loaded with high-density single atoms. Rao et al.[93] demonstrated a versatile and efficient "plasma bombing" strategy for the preparation of SAC-Fe/NC catalysts. In order to create isolated SAC-M/NC catalysts (M = Fe, Mn, Ni, etc.), surface metal salts were driven to evaporate and generate metal single atoms (Figure 7d). HAADF-STEM EDS images show that the carbon supports are evenly distributed with Fe and N elements (Figure 7e). Figure 7f confirms that the Fe atom forms a structure with the coordination of four pyridine N atoms. These atoms were then trapped and adsorbed by the defect sites and nitrogen-containing sites of carbon supports. The strategy proved to be simple, effective, adjustable, and capable of mass production. For the first time, Rao et al.[94] created a straightforward, effective, and adaptable plasma-etching technique to create a range of SACs by merely changing metal precursors and supports (Figure 7g). As shown in Figure 7h,i, the local configuration of the Cu atom in the prepared catalyst can be consistent with the model of CuN_3. Furthermore, the suggested approach is easily scalable to gram-level production, allowing SACs to be used in real-world applications.

Here we introduce seven rapid heating synthesis strategies: pulsed discharge method, graphitic diyne-assisted ultrafast spark synthesis, electro-flash technique, one-step laser implant strategy, one-step thermal breakdown of molten salts, MGB technique, and adaptable plasma-etching technique. These strategies have the characteristics of simple route, high efficiency and maneuverability, which are helpful to quickly construct SACs with special coordination structures and expand the industrial application range of SACs.

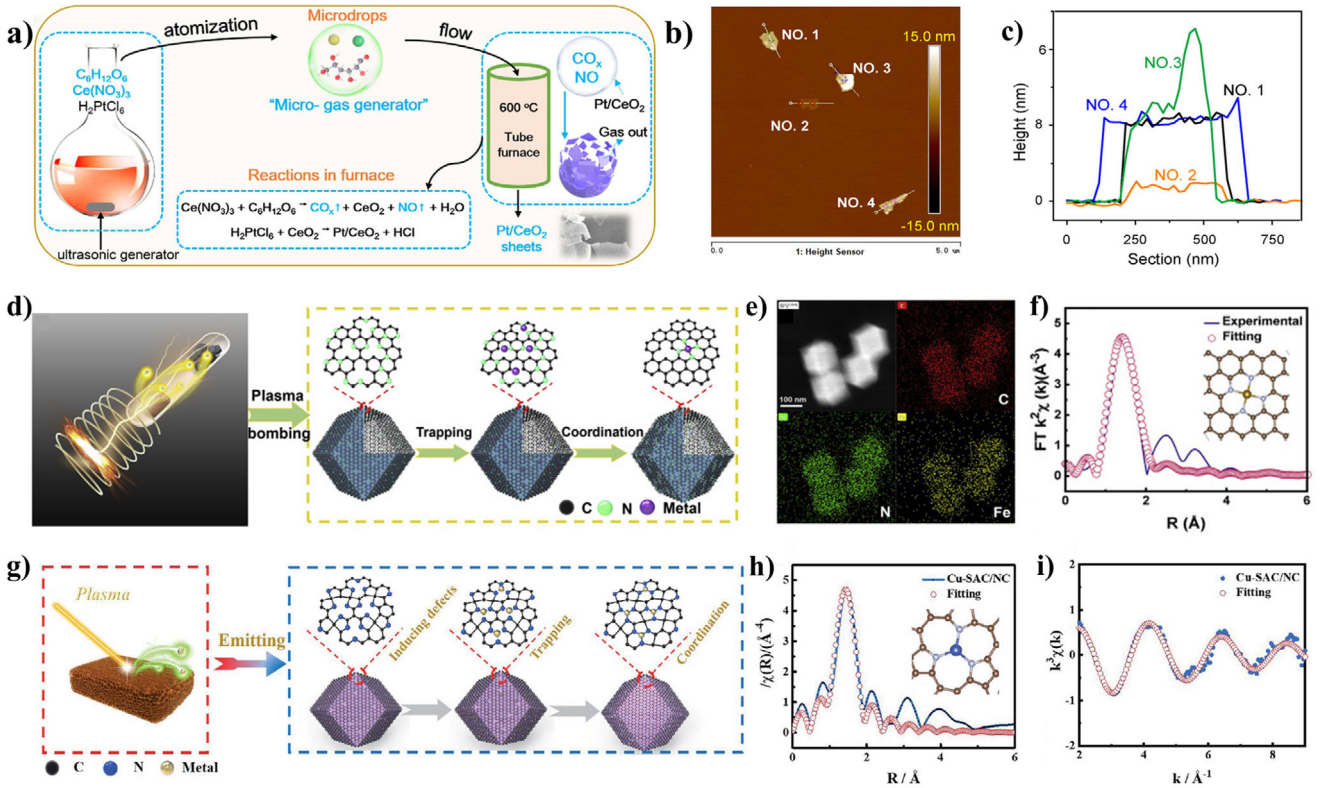

Figure 7. a) Schematic illustration of the MGB method. b) AFM image of Pt_1/CeO_2-S. c) Height distribution of Pt_1/CeO_2-S. Reproduced with permission.[92] Copyright 2022, John Wiley and Sons. d) Schematic diagram of the "plasma bombing" approach. e) HAADF-STEM of SAC-Fe/NC and EDS mapping images. f) The theoretical structure of SAC-Fe/NC and the fitting curve of FT-EXAFS. Reproduced with permission.[93] Copyright 2022, Elsevier. g) Schematic diagram of plasma-etching technique. h) FT-EXAFS fitting curve of Cu-SAC/NC and theoretical structure. i) Cu K-edge EXAFS spectra with K3-weighted of Cu-SAC/NC. Reproduced with permission.[94] Copyright 2022, Royal Society of Chemistry.

In summary, we comprehensively analyzed a variety of ultrafast synthesis methods for the preparation of single-atom catalysts. We summarize the characteristics of the above methods in detail in **Table 1**.

3. Single-Atom Catalysts for Electrocatalytic Applications

3.1. The Electrochemical Carbon Dioxide Reduction Reaction

Removing and sequestering carbon dioxide is an ideal way to address environmental concerns and energy challenges with increasing CO_2 levels around the world. In the CO_2RR, a variety of valuable products can be obtained by transferring 2, 4, 6, 8, or 12 electrons. The most common products are carbon monoxide (CO), methane (CH_4), formic acid (HCOOH), and others. However, due to its highly oxidizing nature, the carbon dioxide molecule is highly chemically stable. In addition, the reduction process of CO_2 is challenged by competitive HER, with high thermodynamic and kinetic barriers, and limited selectivity for specific products. Therefore, many researchers have used ultrafast strategies to synthesize excellent single-atom catalysts for CO_2RR. The following are the applications of four ultrafast synthetic strategies methods in CO_2RR, containing Joule heating method, microwave assistance method, pulsed discharge strategy, and continuous plasma bombardment method.[33,36,39,43,95]

According to Xi et al.,[33] Joule heating was used to synthesize carbon-loaded nickel capsules with precisely controlled structures of single-atom (**Figure 8a**). We compared the CO_2RR Faraday efficiency of samples prepared at different potentials (Figure 8b). It is evident that the optimized Ni SACs ($C_{250}Ph_{3.5}Ni$) have good selectivity for CO generation because they show strong FE_{CO} throughout wide application potentials (-0.7 to -1.9 V vs RHE). The main reason for this is the exclusion of unfavorable N species. When these disadvantageous N species are absent from Ni SACs, competitive HER during CO_2RR may be inhibited. As shown in Figure 8c, after 48 h of reaction at -1.5 V versus RHE, the current density remains stable and FE_{CO} decreases negligibly, indicating perfect stability. Wen et al.[95] developed a rapid pyrolysis method with microwave assistance that provides SAC based on carbon without inert gas protection within 3 min (Figure 8d). Ni_1-N-C-50 has the lowest Tafel slope of 83 mV dec^{-1} compared to the other catalysts in Figure 8e, so the catalyst has good catalytic activity. Figure 8f shows a flow cell device equipped with a gas diffusion electrode (GDE). In Figure 8g, the electrochemical reduction efficiency of Ni_1-N-C-50 reached 1.06 A cm^{-2} and the FE_{CO} was 96%, which far exceeded the electrochemical reduction efficiency of Ni_1-N-C-50 prepared by the traditional pyrolysis method (0.23 A cm^{-2}, FE_{CO} was 93%). According to mechanistic

Table 1. Summary of the characteristics of the ultrafast synthesis method.

Catalysts	Preparation methods	Processing times	Conditions of methods	Refs.
Pt SASs/AG	Microwave reduction	2 min	800 W microwave	[37]
Fe-N-G/CNT	Microwave heating	45 s	800 W microwave	[38]
PSB-CuN_3	Microwave heating	1 s	1000 W microwave	[39]
CuN_1O_1 SAs/GAs	Pulsed discharge	10700 μs	peak value of the current is ≈60 kA.	[43]
Pt_1-FeOx/CN	Electrical pulse	1 s	current of 13.7 A and voltage of 15.3 V	[44]
Co-HGDY	Graphitic diyne-assisted ultrafast spark synthesis	8 ms	3286 K	[45]
CoNG-JH	Joule heating	2 s	–	[67]
Fe-N-DCSs	Joule heating	1 s / 2 s	1200 °C	[68]
Ni_3FeN-Ru_{buried}	Joule heating	2 s	direct current parameterswere set as 5 V 10A	[69]
P-FeN_4@CNTs	Flash Joule heating	200 ms	temperature of 3535 K and cooling rates of 10^4 K s^{-1}	[74]
Co/N-C(PA) and Co/N-C(SP)	Continuous plasma arc (PA method) or Intermittent spark pulse (SP method)	1 min	PA: direct current of 20 kV SP: ~4 pulse per second	[88]
Pt SAs	Laser Planting	5 ns	room-Temperature, fluence of 5.0 J/cm^2 and frequency of 35 kHz at the travelling speed of 1000 mm s^{-1}.	[89]
Ir_1-Co_3O_4 and Pt_1-Co_3O_4	One-step thermal decomposition of molten salts	–	220—300 °C	[91]
Pt_1/CeO_2-S	Micro-gas blasting	0.5 h	200 °C	[92]
SAC-Fe/NC	Plasma bombing	40 min	400 °C and radio frequency power of 500 W	[93]
Cu-SAC/NC	Plasma-etching	40 min	800 °C and radio frequency power of 500 W	[94]

research, carbon defect and mesoporous construction of Ni_1-N-C-50 significantly enhance CO_2 activation and mass transfer capabilities during the catalytic process, producing a high current density.

The above study mentioned that Liu et al.[43] prepared a graphene aerogel-anchored copper single-atom catalyst by pulsed discharge. As shown in Figure 8h, the CO_2RR performance of the catalyst was tested at industrial currents using a flow cell of GDE. In Figure 8i, the unsaturated Cu-N_1O_1 group is linked to the activity and selectivity of formic acid, and an excellent Faradaic efficiency (93.7%) is attained at -0.9 V versus RHE. As shown in Figure 8j, CuN_1O_1 SA/GAs can maintain about FE of 86% in a stability test of -0.9 V versus RHE for 10 h. CuN_1O_1 SA/GAs have 92.5% FE_{HCOO} and are more than 2 times that of CuN_4 SA/GAs, at -0.9 V versus RHE (Figure 8k). Jia et al.[36] reported the process of N doping removal that can be easily achieved under continuous plasma bombardment (Figure 8l). Coordination reconfiguration due to NV can improve catalytic performance. In Figure 8m, the SA-NiNG-NV current density is higher than that of the SA-NiNG and the starting potential is low. For CO_2RR, Ni atoms anchored on extremely faulty N-doped graphene catalysts exhibit excellent stability and high activity. According to mechanistic research, the highly defective pyridinic nitrogen environment lowers the activation energy for the synthesis of the intermediary products COOH* and CO* by offering a large number of vacancies for CO_2 bonding. Dong et al.[39] used microwave heating to create a planar symmetry-broken CuN_3 (PSB-CuN_3) SACs for electrocatalytic CO_2 reduction. As shown in Figure 8n, the CO_2RR performance of PSB-CuN_3 is similar to that of the best catalyst ever reported. In Figure 8o, PSB-CuN_3 had a product selectivity of 94.3% for formic acid at -0.73 V versus RHE. However, the CuN_4 catalyst showed a selectivity of 72.4% at -0.93 V versus RHE. During 100 h of operation, a flow cell using PSB-CuN_3 electrodes maintained a formate selectivity of over 90%.

3.2. The Electrode for the Hydrogen Evolution Reaction

One of the ultimate clean energy carriers is hydrogen. Water splitting reactions are largely dependent on the discovery of inexpensive and high catalytic activity catalysts for HER. In alkaline or acidic media, the evolutionary steps of HER are similar. The first step of HER is to Volmer with H_3O^+ in an acidic medium to form H*, and in an alkaline medium to Volmer with H_2O to form H*. The second step is the rate-determining step, which depends on the activity of these catalysts. For example, in Pt-based catalysts, Tafel reactions adsorb H* to form H_2, while transition metal catalysts typically react H_2O (basic) or H_3O^+ (acidic) with H* to form H_2. Excellent electrocatalytic performance for HER and OER has been demonstrated by SACs made using a variety of techniques. The following are the applications of three ultrafast synthetic strategies methods in HER, containing laser-induced solid-phase method, microwave reduction strategy and transient heating-quenching method,[37,67,96]

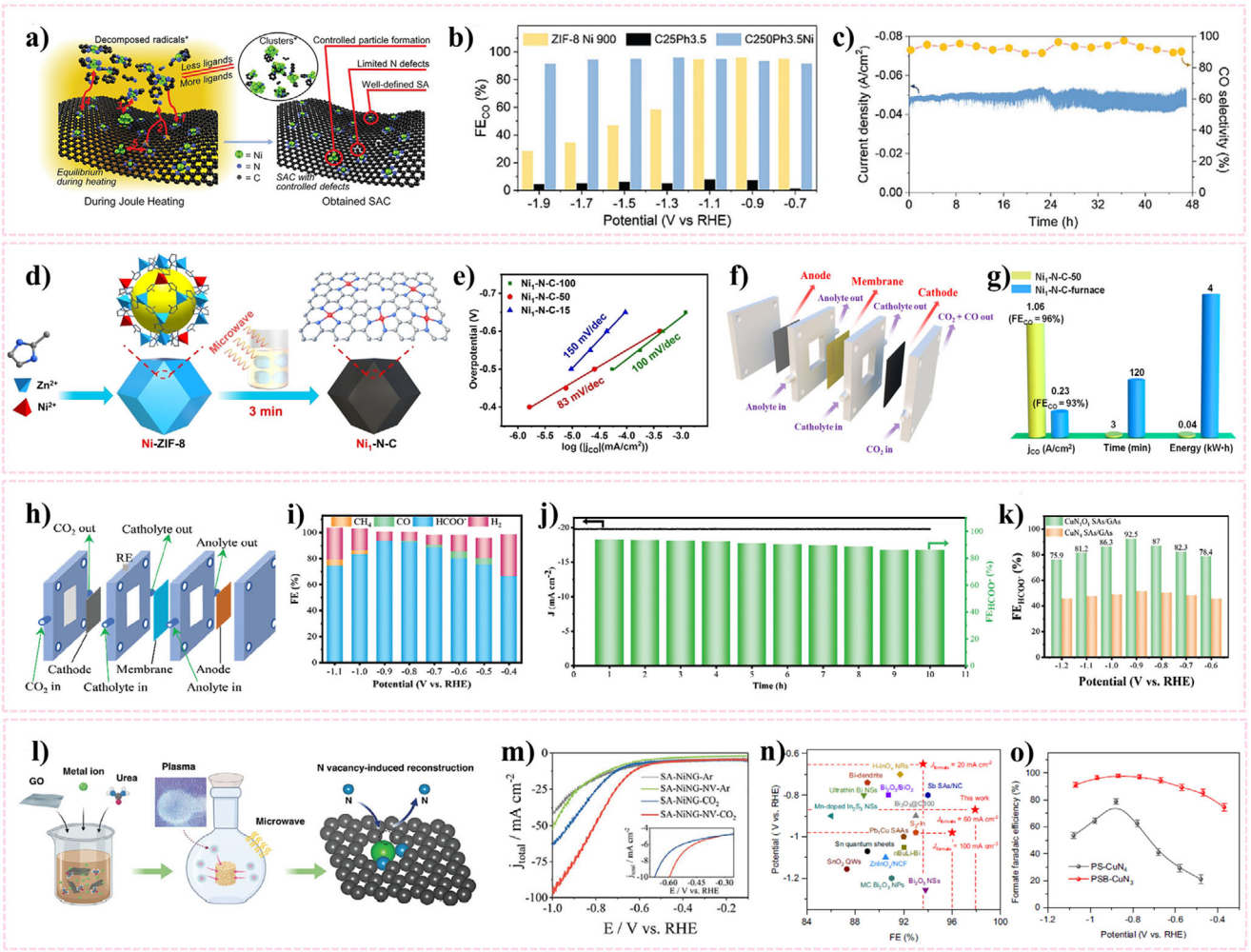

Figure 8. a) Schematic diagram of joule heating approach for synthesis of Ni SACs. b) Faradaic efficiency for the production of CO in various samples. c) Stability of $C_{250}Ph_{3.5}$Ni SAC under -1.5 V versus RHE. Reproduced with permission.[33] Copyright 2021, John Wiley and Sons. d) Schematic diagram of micro-wave-assisted rapid pyrolysis method. e) Tafel plots of Ni_1-N-C-15, Ni_1-N-C-50, and Ni_1-N-C-100. f) Flow cell for CO_2RR diagram with gas diffusion electrode. g) The j_{CO}, time, and energy consumption of Ni_1-N-C-50 and Ni_1-N-C -furnace. Reproduced with permission.[95] Copyright 2024, John Wiley and Sons. h) Schematic illustration of the flow cell. i) The FEs of diverse products for CuN_1O_1 SAs/GAs at different potentials. j) Long-term stability test of CuN_1O_1 SAs/GAs at −0.9 V versus RHE. k) Faradaic efficiency of $HCOO^-$ production. Reproduced with permission.[43] Copyright 2024, John Wiley and Sons. l) Diagram of SAC synthesis using microwave-induced plasma assistance. m) Linear sweep voltammetry (LSV) curves with a scan rate of 20 mV s^{-1}. The inset shows the LSV curve from -0.3 to -0.7 V versus RHE. Reproduced with permission.[36] Copyright 2021, John Wiley and Sons. n) Summary of formate FEs and overpotential of PSB-CuN_3 and various catalysts. o) The formate FEs in different potentials. Reproduced with permission.[39] Copyright 2023, Springer Nature.

As mentioned above, Peng et al.[96] created a laser-induced solid-phase method to synthesize Pt SACs on graphene supports (**Figure 9a**). Pt_5-LrEGO has stable HER performance compared to other catalysts, tested at 10 mA cm^{-2} during 10 h (Figure 9b). In the HER, Pt_5-LrEGO has a mass activity of 12.36 mA μg^{-1} at 50 mV (Figure 9c). In Figure 9d, the Nyquist curve shows that Pt_5-LrEGO exhibits a lower charge transfer resistance (9.88 Ω). Ye et al.[37] prepared aniline-stacked graphene with Pt atoms attached (Pt SASs/AG) with superior HER characteristics using the microwave reduction process. Pt SASs/AG has an excellent HER activity (Figure 9e). The results of the calculation of the Tafel slope of Pt SAS/AG (29.33 mV dec^{-1}) are similar to that of Pt/C (Figure 9f). As shown in Figure 9g, Pt SAS/AG can maintain good stability. In Figure 9h, it is shown that the Pt atom exhibits good HER activity after coordination with aniline. The overpotential is 12 mV at 10 mA cm^{-2} and the mass current density is 22400 at $\eta = 50$ mV. And Pt SASs/AG are more stable and active. Xing et al.[67] developed a transient heating-quenching method for the synthesis of nitrogen-doped graphene-supported single-atom cobalt materials (CoNG-JH). When utilized directly as an electrode for catalytic HER, CoNG-JH shows a current density of 10 mA cm^{-2} and a low overpotential of 106 mV. In the 0.5 M H_2SO_4, it shows long-term durability and a small Tafel slope of 66 mV·dec^{-1} (Figure 9j,k). Figure 9l shows a stability test during 48 h at 10 mA cm^{-2}. The test results show that CoNG-JH has good stability.

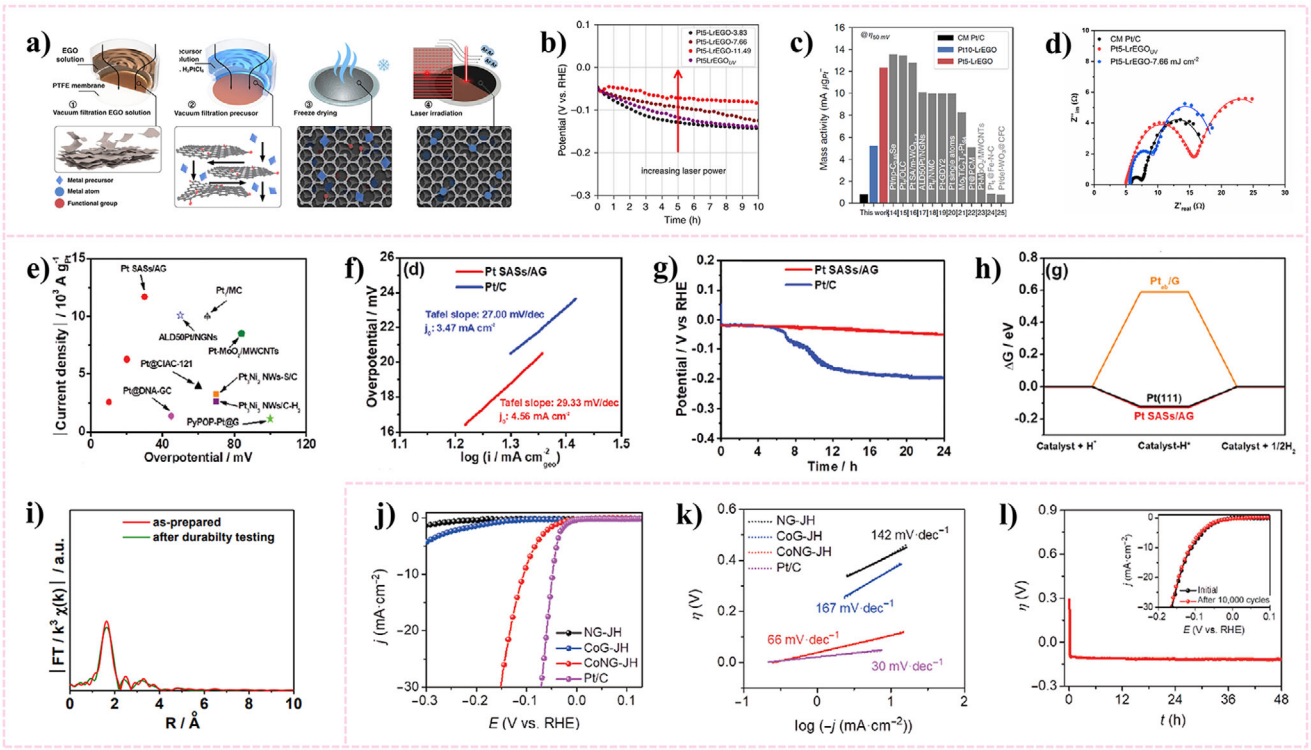

Figure 9. a) Schematic illustration of the formation of Pt-LrEGO. b) Pt-LrEGO sample chromatopotentiometry at different laser fluences with a current density of 10 mA cm^{-2}. c) Mass activity at an overpotential of 50 mV compared to Pt-LrEGO and reference. d) The Nyquist plots of Pt_5-LrEGO, Pt_5-LrEGOUV, and the commercial Pt/C. Reproduced with permission.[96] Copyright 2021, Springer Nature. e) Compared to mass activity of Pt SASs/AG and references in 0.5 M H_2SO_4. f) Pt SASs/AG and Pt/C Tafel plots. g) Pt SASs/AG and Pt/C chronopotentiometric curves in 0.5 M H_2SO_4 solution at 10 mA cm^{-2}. h) HER free energy diagrams were computed for Pt SASs/AG, Pt (111), and P_{tab}/G. Reproduced with permission.[37] Copyright 2019, Royal Society of Chemistry. i) Pt L_3-edge FT-EXAFS of t Pt SASs/AG. j) LSV curves of CoG-JH, NG-JH, CoNG-JH, and 20 wt.% Pt/C. k) Tafel slopes of CoG-JH, NG-JH, CoNG-JH and Pt/C. l) η-t curve of CoNG-JH at 10 mA cm^{-2} within 48 h. Reproduced with permission.[67] Copyright 2021, Springer Nature.

3.3. The Electrode for Oxygen Reduction Reaction and Oxygen Evolution Reaction

ORR is a reaction in which oxygen is reduced to water or other simple oxides by the action of an electrocatalyst on the surface of an electrode. The reaction usually occurs in two halves of an ORR, where the oxygen molecules are reduced to an ionic state on the electrode surface, and then these oxygen species are further involved in the reaction to produce water or other oxides. OER is an important half-reaction in electrochemical energy conversion devices such as electrolysis of water and metal-air batteries. The first step of OER under acidic conditions is the dissociation of water, and the final products are H^+ and O_2. The first step of OER under alkaline conditions is the adsorption of OH^-, and the final products are H_2O and O_2. The following are the applications of six ultrafast synthetic strategies methods in ORR and OER, containing one-step microwave thermal shock method, novel flash heating (FH) strategy, flash-thermal shock (FTS) strategy, plasma bombing approach, microwave heating and electrospinning method, and brief heat treatment procedure.[93,97–101]

The oxygen reduction reaction, which produces H_2O_2 electrochemically, is a viable substitute for the energy-intensive anthraquinone process. Gong et al.[97] created a one-step microwave thermal shock method for synthesis of SACs (**Figure 10a**). This method enables concurrently modify the coordination number of the adjacent oxygen functional group and the atomically scattered cobalt site, creating Co-N-C electrocatalysts with high selectivity and activity for H_2O_2 electrosynthesis. Co-N_2-C/HO exhibits the better activity than standard Co-N_4-C/LO SACs. Figure 10b–d demonstrates that Co-N_2-C/HO has a high H_2O_2 selectivity (91.3%) and a kinetic current density of 11.3 mA cm^{-2} at 0.65 V. And the mass activity of Co-N_2-C/HO is 44.4 A g^{-1} at 0.65 V, and the start-up potential of Co-N_2-C/HO is 0.801 V. Luo et al.[98] proposed the FH strategy for surface atom adsorption (Figure 10e). As shown in Figure 10f, CoN_5/PCNF has a higher half-wave potential (0.92 V) compared to other materials. Compared with the reported catalysts, CoN_5/PCNF has higher mass activity and conversion frequency (Figure 10g). Since the surface adsorption-FH synthesis method can expose more catalytic sites, the utilization rate of CoN_5/PCNF active sites is improved (Figure 10h). In the OER reaction, CoN_5/PCNF has a small overpotential (270 mV) at 10 mA cm^{-2}. Because the excellent catalytic activity of the new CoN_5 coordination catalyst and the plateau utilization rate work in concert, the TOF of 65.33 s^{-1} was more than 47.4 times that of 20% Pt/C. CoN_5/PCNF exhibited an excellent electrocatalytic activity, good ORR kinetics, and excellent 4-electron selectivity for both OER and ORR. Kim et al.[99] suggested a technique that uses FTS method to anchor metal atoms on N-doped graphene supports in a site-specific. Co SACs_N@rGO has a high activity of ORR (Figure 10j). The average number of electron transfers

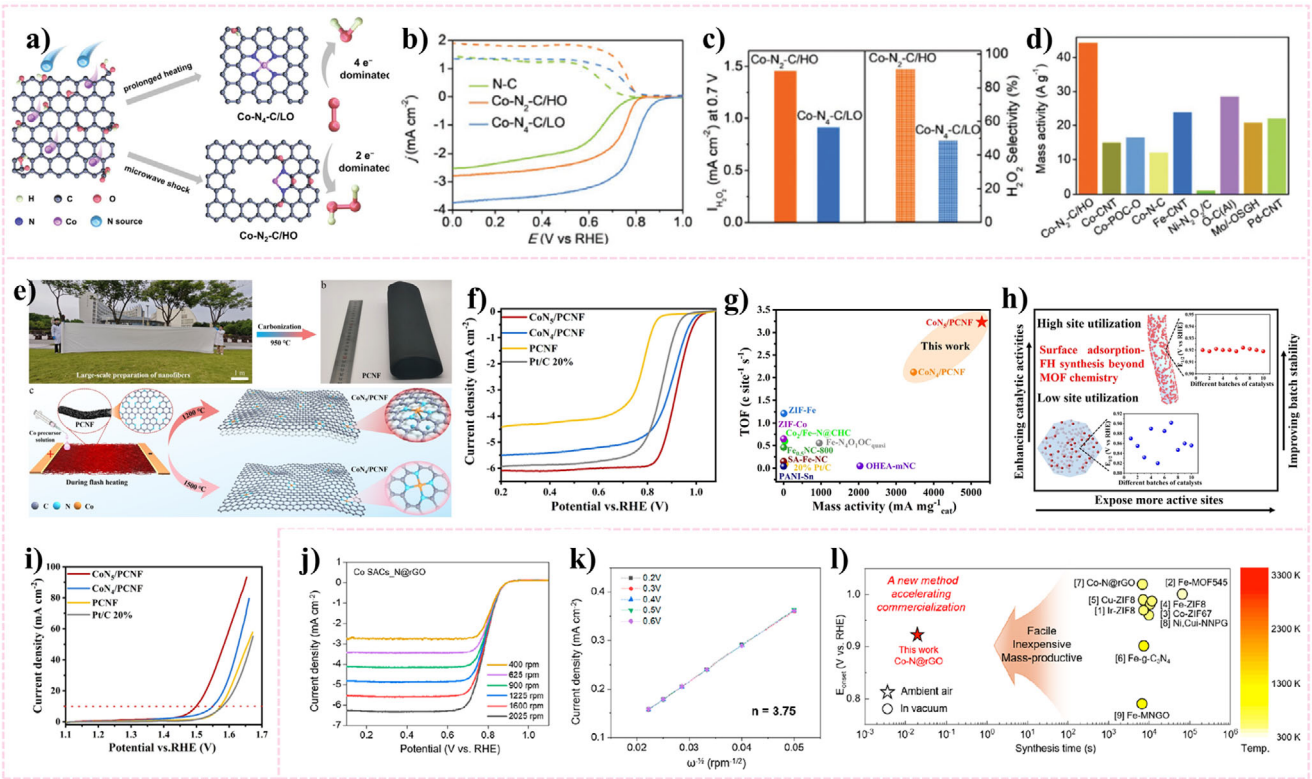

Figure 10. a) Schematic diagram of the synthesis route to Co-N_4-C/LO and Co-N_2-C/HO. b) Rotating ring-disk electrode voltammograms of N-C, Co-N_2-C/HO and Co-N_4-C/LO. c) H_2O_2 selectivity and current comparison for Co-N_2-C/HO and Co-N_4-C/LO at 0.7 V. d) Mass activity at 0.65 V of Co-N_2-C/HO and othe SACs catalysts. Reproduced with permission.[97] Copyright 2022, John Wiley and Sons. e) Schematic diagram of FH strategy for surface atom adsorption. f) ORR polarization curves measured at 1600 rpm and 5 mV s^{-1}. g) Mass activity and TOF values are compared between references, CoN_5/PCNF, and CoN_4/PCNF at 0.9 V versus RHE. h) Surface adsorption-FH beyond delicate metal-organic framework (MOF) chemistry. i) Curves of OER polarization in 1 M KOH. Reproduced with permission.[98] Copyright 2024, John Wiley and Sons. j) LSV curves of Co SACs_N@rGO at different rotation speed. k) The matching J^{-1} versus $\omega^{-1/2}$ K-L plots of Co SACs_N@rGO in the various potentials. l) Summary of ORR properties and synthesis time about single atom in N-doped carbon carriers prepared by different methods. Reproduced with permission.[99] Copyright 2023, American Chemical Society.

produced by Co SACs_N@rGO is 3.75 (Figure 10k). The catalytic performance of Co SAC_N@rGO was equivalent to that of SAC samples prepared by a traditional furnace annealing procedure in a vacuum setting, with an average electron transfer number of 3.75 and a half-wave potential ($E_{1/2}$) of 0.80 V. By analyzing Figure 10l, the synthesis method of FTS may become a commercial option.

Rao et al.[93] explored a plasma bombing approach to prepare SAC-Fe/NC which has a significant ORR performance. **Figure 11**a,b shows that the current density of SAC-Fe/NC is 9.890 mA cm^{-2}, and the high half-wave potential is 0.920 V. Both of SAC-Fe/NC are greater than the current density and half-wave potential of Pt/C and pure NC. Following the accelerated durability test (ADT), there was minimal activity attenuation in terms of $E_{1/2}$ and J_k in addition to the high activity, suggesting that the produced SAC-Fe/NC had exceptional durability (Figure 11c). Zhao et al.[100] reported a technology that uses controlled microwave heating and electrospinning to quickly synthesize a number of atomically distributed transition metal atoms on nitrogen-doped multi-level porous carbon nanofibers (M-TM/NPCNFs, TM = Fe, Co, Ni, FeCo, and FeNi), as shown in Figure 11d. The synthesized M-Fe/NPCNFs-900 demonstrated outstanding ORR activity in alkaline conditions. M-Fe/NPCNFs-900 has an overpotential of 0.85 V, and the J_k is 11.95 mA cm^{-2} (Figure 11e). Figure 11f shows the free energy diagram of the ORR reaction pathway, which can be carried out spontaneously on the surface of the catalyst. Jang et al.[101] presented a new and effective method for creating SACs through a brief heat treatment procedure (Figure 11g). In this method, iron phthalocyanine (FePc) and graphene oxide (GO) were used to rapidly generate FeN_4 catalysts with the optimal structure of basic ORR. Figure 11h shows the Cyclic Voltammetry (CV) curves of four samples at a scan rate of 100 mV s^{-1} and the voltage range of -0.05 to -1.1 V versus RHE. Two characteristic peaks of FeN_4/NGO_0.0 m and FeN_4/NGO_1.0 m were exhibited the redox of the central atom Fe, and it were typical of FePc.[102] The measurement was conducted using RDE at 1600 rpm[103,104] (Figure 11i). FeN_4/NGO_2.5 m is the best catalyst for heat-treated samples. In comparison to standard Pt/C catalysts, FeN_4/NGO_2.5 m exhibits greater performance, ORR activity, and durability.

We summarize the applications of SACs prepared by various ultrafast synthesis strategies. **Table 2** provides an overview of the loadings, preparation procedures, and electrocatalytic uses of single-atom catalysts.

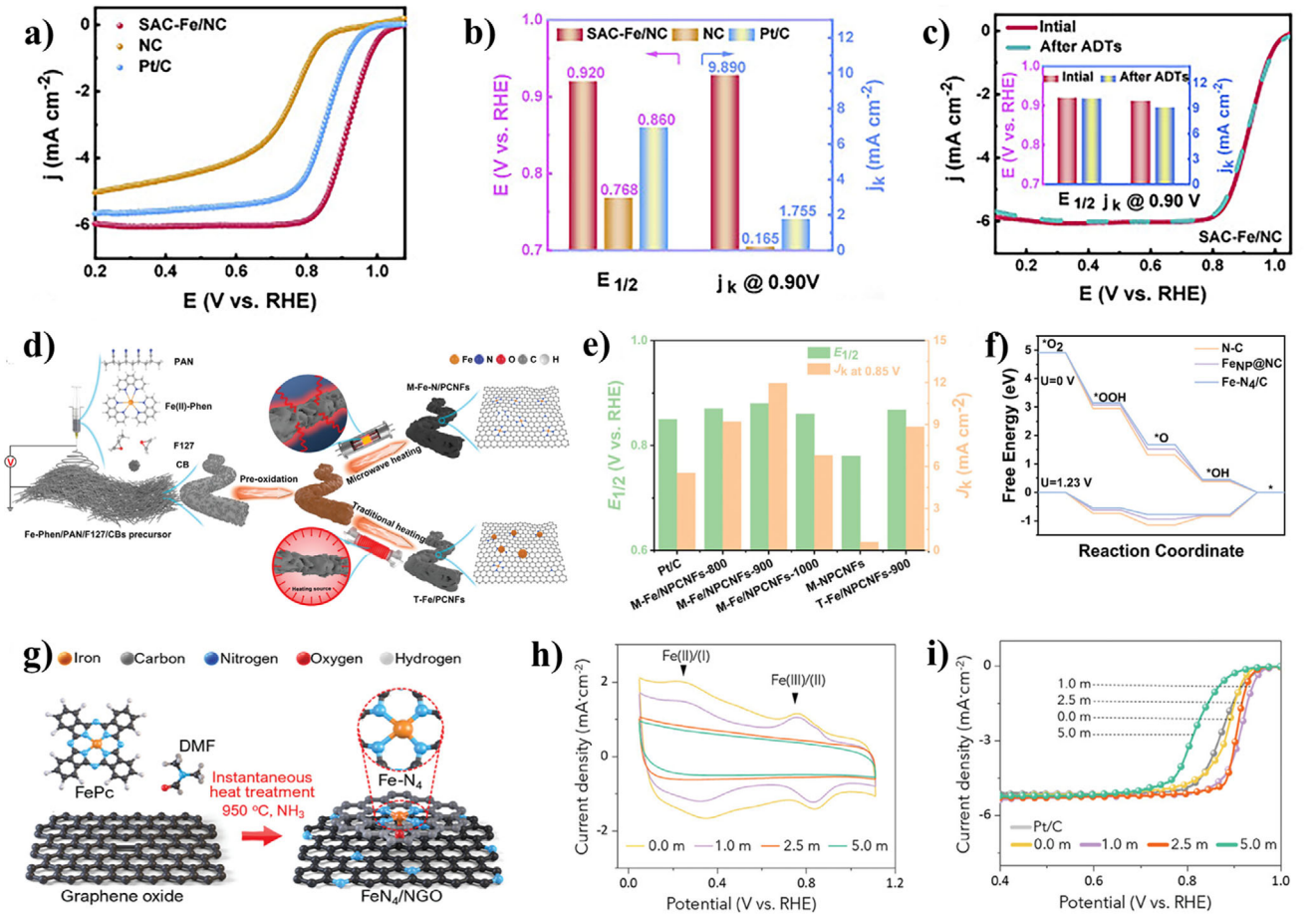

Figure 11. a) LSV curves of NC, Pt/C, and SAC-Fe/NC. b) $E_{1/2}$ and j_k @ 0.90 V of SAC-Fe/NC and references. c) LSV curves, $E_{1/2}$, and j_k of SAC-Fe/NC and SAC-Fe/NC after ADTs. Reproduced with permission.[93] Copyright 2022, Elsevier. d) Illustration of the synthesis route for M-Fe/NPCNFs catalysts. e) Comparison of J_k and $E_{1/2}$ between various catalysts. f) calculated free energy diagrams of the ORR process by calculating for N-C, Fe-N_4/C and Fe_{NP}@NC. Reproduced with permission.[100] Copyright 2024, John Wiley and Sons. g) Simplified diagram of an instantaneous heat treatment process for catalyst synthesis. h) CV curves at 0.05-1.05 V versus RHE and 100 mV s^{-1} in 0.1 M KOH (N_2-saturated). i) Steady-state and iR-free ORR polarization curves. Reproduced with permission.[101] Copyright 2024, John Wiley and Sons.

4. Conclusion

In conclusion, we summarize the synthetic SACs for various ultrafast synthesis strategies and electrocatalytic applications. The traditional methods for the preparation of SACs are difficult to produce on a large scale due to their low yields and complex experimental procedures. They are also limited by shortcomings such as poor generality and long processing time. Compared to the traditional methods, the advantages of a rapid synthesis strategy on instantaneous quenching, rapid heating, and rapid ignition could effectively prevent metal atom migration and aggregation, preserve the stability of isolated atom during the manufacture of SACs. Moreover, the instantaneous quenching during the ultrafast synthesis can facilitate bond formation between the single atom and supports which results in excellent stability in the catalytic process. In addition, methods such as pulsed discharge and Joule heating ensure uniform mixing between the metal and the support and a uniform heat distribution throughout the material, ensuring homogeneity of the synthetic sample. The ultrafast synthesis strategy can often shorten the preparation time of SACs, with high efficiency.

However, the quick heating synthesis approach still has several drawbacks and difficulties when it comes to producing SACs. All of the above strategies have short heating and cooling process durations, which presents challenges for accurate temperature control and measurement. In the above methods, there are few studies on single-atomic materials with high loading, and increasing the high loading capacity may become a research hotspot in the future. In addition, the use of in situ electron microscopy to detect the synthesis mechanism of single atoms in the ultrafast synthesis process may also become a research hotspot. The synthesis mechanism of single atoms detected by in situ X-ray absorption fine structure can also be studied in depth.

SACs have a promising application in the field of electrochemistry. In high-energy environments, the ultrafast synthesis strategy can decrease the exposure of metal atoms. The ultrafast synthesis method can reduce atomic agglomeration and can be beneficial for increasing the loading of metals, which can enhance the electrocatalysis activity of SACs. We summarize that SACs

Table 2. Summary of loading and electrochemical applications of SACs prepared by various methods.

Catalysts	Preparation methods	Mass loading of mental	Electrocatalytic applications	Refs.
Carbon-supported Ni SACs	Joule heating	1.0 wt.%	CO_2RR	[33]
Pt SASs/AG	Microwave reduction	0.44 wt.%	HER	[37]
Fe-N-G/CNT	Microwave heating	1.45 wt.%	ORR	[38]
PSB-CuN_3	Microwave heating	0.48 at.%	CO_2RR	[39]
Co-NG-MW	Microwave heating	1.10 wt.%	HER	[42]
CuN_1O_1 SAs/Gas	Pulsed discharge	1.03 at.%	CO_2RR	[43]
Pt_1-FeOx/CN	Electrical pulse	Pt: 0.21 at.% Fe: 1.11 at.%	ORR	[44]
CoNG-JH	Joule heating	0.81 wt.%	HER	[67]
Fe-N-DCSs	Joule heating	0.682 wt.%	ORR	[68]
P-FeN_4@CNTs	Flash Joule heating	1.487 wt.%	ORR	[74]
Co/N-C(PA) and Co/N-C(SP)	Continuous plasma arc (PA method) or Intermittent spark pulse (SP method)	3.5 wt.% / 0.7 wt.%	ORR	[88]
Pt Sas	Laser Planting	41.8 wt.%	HER	[89]
Ir_1-Co_3O_4 and Pt_1-Co_3O_4	One-step thermal decomposition of molten salts	Ir: 10.97 wt.% Pt: 4.60 wt.%	OER and HER	[91]
Ni_1-N-C	Microwave-assisted rapid pyrolysis	1.3 wt.%~1.6 wt.%	CO_2RR	[95]
Pt-LrEGO	Laser solid-phase	0.41 wt.%	HER	[96]
Co-N-C	One-step microwave thermal shock	0.14 wt.%	ORR	[97]
CoN_5/PCNF and CoN_4/PCNF	Surface atom adsorption-flash heating	1.10 wt.% / 0.85 wt.%	ORR and OER	[98]
Ru_{SA}@$Cu_{2+1}O$	Joule heating	Ru: 2.4 wt.%	NO_3RR	[105]
Ni_2N_6O/NC	Microwave pyrolysis	0.85 wt.%	CO_2RR	[106]

synthesized by ultrafast synthesis methods exhibit excellent catalytic performance. SACs have been widely used in the reactions of HER, ORR, OER, and CO_2RR. It is necessary to continue to explore whether the SACs prepared by the ultrafast synthesis method can be used in other electrocatalytic reactions. Future research should focus on the stabilization improvement of SACs and the application of ultrafast synthesis processes in industry. We should explore the potential of more electrocatalysis by developing new ultrafast synthesis methods. In addition, cross-scale studies can be carried out in combination with theoretical calculations, such as multi-scale and systematic study of the mechanism of ultrafast synthesis processes.

In short, the ultrafast synthesis strategy should be given more attention in the preparation of SACs. And more electrocatalytic applications will be explored. The ultrafast synthesis strategy will create an innovative pathway for the rapid synthesis of SACs with good performance.

Acknowledgements

The authors acknowledge financial support from the National Natural Science Foundation of China (22375019), the China Postdoctoral Science Foundation (2024M764116), the University Natural Science Research Project of Anhui Province (2024AH040186), and the Application Project of Bengbu University (2024YYX28QD).

Conflict of Interest

The authors declare no conflict of interest.

Author Contributions

B.Z. and K.L. contributed equally to this work. All authors have given approval to the final version of the manuscript.

Keywords

electrocatalytic applications, joule heating, microwave heating, pulsed discharge, single-atom catalysts, ultrafast synthesis

Received: February 14, 2025
Revised: March 26, 2025
Published online:

[1] M. K. Debe, *Nature* **2012**, *486*, 43.
[2] B. Zhang, *Science* **2016**, *352*, 333.
[3] I. Roger, M. Shipman, M. Symes, *Nat. Rev. Chem.* **2017**, *1*, 0003.
[4] S. Gao, X. Jiao, Z. Sun, W. Zhang, Y. Sun, C. Wang, Q. Hu, X. Zu, F. Yang, S. Yang, L. Liang, J. Wu, Y. Xie, *Angew. Chem., Int. Ed.* **2016**, *55*, 698.
[5] C. Zhu, S. Guo, S. Dong, *Adv. Mater.* **2012**, *24*, 2326.
[6] M. Boudart, B. H. Davis, H. Heinemann, in *Handbook of Heterogeneous Catalysis*, (Eds: G. Ertl, H. Knözinger, F. Schuth, J. Weitkamp), Wiley-VCH, Weinheim **2008**.
[7] F. Yang, D. H. Deng, X. L. Pan, Q. Fu, X. H. Bao, *Natl. Sci. Rev.* **2015**, *2*, 183.
[8] X. F. Yang, A. Wang, B. Qiao, *Acc. Chem. Res.* **2013**, *46*, 1740.
[9] R. Qin, P. Liu, G. Fu, N. Zheng, *Small Methods* **2018**, *2*, 1700286.
[10] M. Hu, J. Zhang, W. Zhu, *Nano Res.* **2018**, *11*, 905.
[11] L. Liu, A. Corma, *Chem. Rev.* **2016**, *118*, 4981.

[12] C. Z. Wan, X. F. Duan, *Matter* **2019**, *1*, 555.
[13] A. Giugni, *Nat. Nanotechnol.* **2019**, *14*, 814.
[14] Y. G. Yao, *Nat. Nanotechnol.* **2019**, *14*, 851.
[15] C. F. Du, X. L. Sun, H. Yu, W. Fang, Y. Jing, Y. H. Wang, S. Q. Li, X. H. Liu, Q. Y. Yan, *InfoMat* **2020**, *2*, 950.
[16] S. F. J. Hackett, R. M. Brydson, M. H. Gass, I. Harvey, A. D. Newman, K. Wilson, A. F. Lee, *Angew. Chem., Int. Ed.* **2007**, *46*, 8593.
[17] Y. X. Chen, Z. W. Huang, Z. Ma, J. M. Chen, X. F. Tang, *Catal. Sci. Technol.* **2017**, *7*, 4250.
[18] B. J. O'Neill, D. H. K. Jackson, J. Lee, C. Canlas, P. C. Stair, C. L. Marshall, J. W. Elam, T. F. Kuech, J. A. Dumesic, G. W. Huber, *ACS Catal.* **2015**, *5*, 1804.
[19] N. C. Cheng, X. L. Sun, *Chin. J. Catal.* **2017**, *38*, 1508.
[20] J. Wang, Z. J. Li, Y. E. Wu, Y. D. Li, *Adv. Mater.* **2018**, *30*, 1801649.
[21] S. F. Ji, Y. J. Chen, X. L. Wang, Z. D. Zhang, D. S. Wang, Y. D. Li, *Chem. Rev.* **2020**, *120*, 11900.
[22] Y. F. Hu, H. X. Li, Z. S. Li, B. L. Li, S. Y. Wang, Y. C. Yao, C. L. Yu, *Green Chem.* **2021**, *23*, 8754.
[23] A. Q. Wang, J. Li, T. Zhang, *Nat. Rev. Chem.* **2018**, *2*, 65.
[24] Y. X. Wang, *Chem. Rev.* **2020**, *120*, 12217.
[25] Y. F. Ma, B. L. Chi, W. Liu, L. N. Cao, Y. Lin, X. H. Zhang, X. X. Ye, S. Q. Wei, J. L. Lu, *ACS Catal.* **2019**, *9*, 8404.
[26] R. X. Qin, K. L. Liu, Q. Y. Wu, N. F. Zheng, *Chem. Rev.* **2020**, *120*, 11810.
[27] Y. G. Yao, *Nat. Nanotechnol.* **2019**, *14*, 851.
[28] Y. G. Yao, *Science* **2018**, *359*, 1489.
[29] Q. Y. Bi, X. T. Yuan, Y. Lu, D. Wang, J. Huang, R. Si, M. L. Sui, F. Q. Huang, *Research* **2020**, *2020*, 9140841.
[30] D. Jiang, *Angew. Chem., Int. Ed.* **2021**, *60*, 26054.
[31] Q. Lu, H. Wu, X. R. Zheng, Y. N. Chen, A. L. Rogach, X. P. Han, Y. D. Deng, W. B. Hu, *Adv. Sci.* **2021**, *8*, 2101438.
[32] J. Y. Du, G. Wu, K. Liang, J. Yang, Y. D. Zhang, Y. Lin, X. S. Zheng, Z. Q. Yu, Y. E. Wu, X. Hong, *Small* **2021**, *17*, 2007264.
[33] D. W. Xi, *Adv. Mater.* **2021**, *34*, 2104090.
[34] H. S. Gong, *Adv. Funct. Mater.* **2022**, *32*, 2106886.
[35] R. W. Meng, *Adv. Energy Mater.* **2021**, *11*, 2100683.
[36] C. Jia, *Adv. Funct. Mater.* **2021**, *31*, 2107072.
[37] S. H. Ye, *Energy Environ. Sci.* **2019**, *12*, 1000.
[38] R. Meng, C. Zhang, Z. Lu, X. Xie, Y. Liu, Q. Tang, H. Li, D. Kong, C. N. Geng, Y. Jiao, Z. Fan, Q. He, Y. Guo, G. Ling, Q. H. Yang, *Adv. Energy Mater.* **2021**, *11*, 2100683.
[39] J. Dong, Y. Liu, J. Pei, *Nat. Commun.* **2023**, *14*, 6849.
[40] W. Y. Noh, E. M. Kim, K. Y. Kim, J. H. Kim, H. Y. Jeong, P. Sharma, G. Lee, J. W. Jang, S. H. Joo, J. S. Lee, *J. Mater. Chem. A* **2020**, *8*, 18891.
[41] Q. D. Li, *ACS Appl. Energy Mater.* **2020**, *3*, 8266.
[42] H. L. Fei, *Adv. Mater.* **2018**, *30*, 1802146.
[43] K. Y. Liu, Z. Y. Sun, W. X. Chen, X. F. Lang, X. Gao, P. W. Chen, *Adv. Funct. Mater.* **2024**, *34*, 2312589.
[44] C. L. Ye, M. Zheng, Z. M. Li, Q. K. Fan, H. Q. Ma, X. Z. Fu, D. S. Wang, J. Wang, Y. D. Li, *Angew. Chem., Int. Ed.* **2022**, *134*, 51.
[45] X. Zheng, X. Gao, R. A. Vilá, *Nat. Nanotechnol.* **2023**, *18*, 153.
[46] K. M. Wyss, D. X. Luong, J. M. Tour, *Adv. Mater.* **2022**, *34*, 2106970.
[47] J. Liu, *ACS Catal.* **2017**, *7*, 34.
[48] S. Sun, G. Zhang, N. Gauquelin, N. Chen, J. Zhou, S. Yang, W. Chen, X. Meng, D. Geng, M. N. Banis, R. Li, S. Ye, S. Knights, G. A. Botton, T. K. Sham, X. Sun, *Sci. Rep.* **2013**, *3*, 1775.
[49] X. Zhang, J. Guo, P. Guan, C. Liu, H. Huang, F. Xue, X. Dong, S. J. Pennycook, M. F. Chisholm, *Nat. Commun.* **2013**, *4*, 1924.
[50] J. Deng, H. Li, J. Xiao, Y. Tu, D. Deng, H. Yang, H. Tian, J. Li, P. Ren, X. Bao, *Energy Environ. Sci.* **2015**, *8*, 1594.
[51] C. K. Poh, S. H. Lim, J. Lin, Y. P. Feng, *J. Phys. Chem. C* **2014**, *118*, 13525.
[52] Z. Zhang, X. Gao, M. Dou, J. Ji, F. Wang, *Small* **2017**, *13*, 1604290.
[53] B. Bayatsarmadi, Y. Zheng, A. Vasileff, S. Z. Qiao, *Small* **2017**, *13*, 1700191.
[54] C. E. Creissen, M. Fontecave, *Nat. Commun.* **2022**, *13*, 2280.
[55] L. Guo, J. W. Zhou, F. Liu, X. Meng, Y. B. Ma, F. K. Hao, Y. C. Xiong, Z. X. Fan, *ACS Nano* **2024**, *18*, 9823.
[56] P. Kumar, K. Kannimuthu, A. S. Zeraati, S. Roy, X. Wang, X. Y. Wang, *J. Am. Chem. Soc.* **2023**, *145*, 8052.
[57] S. Iqbal, B. Safdar, I. Hussain, K. Zhang, C. Chatzichristodoulou, *Adv. Energy Mater.* **2023**, *13*, 2203913.
[58] F. Jiang, Y. Li, Y. Pan, *Adv. Mater.* **2024**, *36*, 2306309.
[59] W. Yang, P. Cheng, Z. Li, Y. Lin, M. Li, J. Zi, H. Shi, G. Li, Z. Lian, H. Li, *Adv. Funct. Mater.* **2022**, *32*, 2205920.
[60] Y. Li, X. Liu, J. Xu, S. Chen, *Small* **2024**, *20*, 2402846.
[61] C. Wan, X. Duan, Y. Huang, *Adv. Energy Mater.* **2020**, *10*, 1903815.
[62] M. Liu, J. Zhang, H. Su, *Nat. Commun.* **2024**, *15*, 1675.
[63] C. Li, Z. Wang, M. Liu, *Nat. Commun.* **2022**, *13*, 3338.
[64] J. Yoon, Y. Kim, J. Song, *J. Mater. Chem. A* **2023**, *11*, 22295.
[65] Y. Yao, *Science* **2018**, *359*, 1489.
[66] S. Wang, Q. Liu, S. Li, F. Huang, H. Zhang, *ACS Nano* **2024**, *18*, 5040.
[67] L. Xing, R. Liu, Z. Gong, *Nano Res.* **2022**, *15*, 3913.
[68] Y. Liu, L. Zong, Y. Zhang, F. Lu, L. Wang, *Appl. Catal., B* **2025**, *361*, 124673.
[69] Y. Lin, B. Geng, R. Zheng, *Nat. Commun.* **2025**, *16*, 286.
[70] J. Du, Y. Zhang, H. Lv, A. Chen, *J. Colloid Interface Sci.* **2021**, *587*, 780.
[71] D. Xi, J. Li, J. Low, K. Mao, R. Long, J. Li, Z. Dai, T. Shao, Y. Zhong, Y. Li, Z. Li, X. J. Loh, L. Song, E. Ye, Y. Xiong, *Adv. Mater.* **2021**, *34*, 2104090.
[72] Y. Qiu, Z. Hu, H. Li, Q. Ren, Y. Chen, S. Hu, *Chem. Eng. J.* **2022**, *430*, 132769.
[73] D. Xia, J. Mannering, P. Huang, Y. Xu, Q. Li, H. Li, Y. Qin, A. N. Kulak, R. Menzel, *J. Am. Chem. Soc.* **2023**, *146*, 159.
[74] G. B. Qin, S. D. Sun, X. H. Zhang, Z. Han, Y. P. Li, G. Y. Han, Y. Li, S. Zhu, *Energy Storage Mater.* **2024**, *69*, 2405.
[75] F. Kishimoto, T. Yoshioka, R. Ishibashi, H. Yamada, K. Muraoka, H. Taniguchi, T. Wakihara, K. Takanabe, *Sci. Adv.* **2023**, *9*, 1744.
[76] X. Wu, Z. Wang, D. Zhang, Y. Qin, M. Wang, Y. Han, T. Zhan, B. Yang, S. Li, J. Lai, L. Wang, *Nat. Commun.* **2021**, *12*, 4018.
[77] C. Jia, S. Li, Y. Zhao, R. K. Hocking, W. Ren, X. Chen, Z. Su, W. Yang, Y. Wang, S. Zheng, F. Pan, C. Zhao, *Adv. Funct. Mater.* **2021**, *31*, 2107072.
[78] H. Fei, J. Dong, C. Wan, Z. Zhao, X. Xu, Z. Lin, Y. Wang, H. Liu, K. Zang, J. Luo, S. Zhao, W. Hu, W. Yan, I. Shakir, Y. Huang, X. Duan, *Adv. Mater.* **2018**, *30*, 1802146.
[79] F. Bu, W. Chen, J. Gu, P. O. Agboola, N. F. Al-Khalli, I. Shakir, Y. Xu, *Chem. Sci.* **2018**, *9*, 7009.
[80] S. Głowniak, B. Szczęśniak, J. Choma, M. Jaroniec, *Adv. Mater.* **2021**, *33*, 2103477.
[81] H. Qiao, M. T. Saray, X. Wang, S. Xu, G. Chen, Z. Huang, C. Chen, G. Zhong, Q. Dong, M. Hong, H. Xie, R. Shahbazian-Yassar, L. Hu, *ACS Nano* **2021**, *15*, 14928.
[82] R. Meng, C. Zhang, Z. Lu, X. Xie, Y. Liu, Q. Tang, H. Li, D. Kong, C. N. Geng, Y. Jiao, Z. Fan, Q. He, Y. Guo, G. Ling, Q. H. Yang, *Adv. Energy Mater.* **2021**, *11*, 2100683.
[83] J. Dong, Y. Liu, J. Pei, *Nat. Commun.* **2023**, *14*, 6849.
[84] A. Mansour, J. Cook Jr, D. Sayers, *J. Phys. Chem.* **1984**, *88*, 2330.
[85] T. Sham, S. Naftel, I. Coulthard, *J. Appl. Phys.* **1996**, *79*, 7134.
[86] H. Fei, *Nat. Catal.* **2018**, *1*, 63.
[87] C. Li, R. Han, J. Bai, Y. Cao, W. Yuan, J. Wu, P. Li, X. Chen, *Carbon* **2023**, *213*, 118296.
[88] J. Du, G. Wu, K. Liang, J. Yang, Y. Zhang, Y. Lin, X. Zheng, Z. Q. Yu, Y. Wu, X. Hong, *Small* **2021**, *17*, 2007264.
[89] B. Wang, X. Zhu, X. D. Pei, W. G. Liu, Y. C. Leng, X. W. Yu, C. Wang, L. H. Hu, Q. M. Su, C. P. Wu, Y. F. Yao, Z. Q. Lin, Z. G. Zou, *J. Am. Chem. Soc.* **2023**, *145*, 13788.

[90] Y. Xia, R. Luo, Y. Fu, Y. Pan, W. Hao, J. Fan, Q. Bi, G. Li, *Adv. Funct. Mater.* **2024**, *34*, 2408300.
[91] S. Kaushik, D. Wu, Z. Zhang, X. Xiao, C. Zhen, W. Wang, N. Y. Huang, M. Gu, Q. Xu, *Adv. Mater.* **2024**, *36*, 2401163.
[92] L. Kuai, L. Liu, Q. M. Tao, N. Yu, E. J. Kan, N. Sun, S. J. Liu, B. Y. Geng, *Angew. Chem., Int. Ed.* **2022**, *61*, 202212338.
[93] P. Rao, D. X. Wu, J. M. Luo, J. Li, P. L. Deng, Y. J. Shen, X. L. Tian, *Cell Rep. Phys. Sci.* **2022**, *3*, 100880.
[94] P. Rao, D. X. Wu, Y. Y. Qin, J. M. Luo, *J. Mater. Chem. A* **2022**, *10*, 6531.
[95] M. Wen, N. Sun, L. Jiao, S. Q. Zang, H. L. Jiang, *Angew. Chem., Int. Ed.* **2024**, *63*, 202318338.
[96] Y. Peng, J. Cao, Y. Sha, *Light: Sci. Appl.* **2021**, *10*, 168.
[97] H. Gong, Z. Wei, Z. Gong, J. Liu, G. Ye, M. Yan, J. Dong, C. Allen, J. Liu, K. Huang, R. Liu, G. He, S. Zhao, H. Fei, *Adv. Funct. Mater.* **2022**, *32*, 2106886.
[98] Q. Luo, K. Wang, Q. Zhang, W. Ding, R. Wang, L. Li, S. Peng, D. Ji, X. Qin, *Angew. Chem., Int. Ed.* **2024**, *64*, 202413369.
[99] D. H. Kim, J. H. Cha, S. Chong, S. H. Cho, H. Shin, J. Ahn, D. Jeon, J. Kim, S. Y. Choi, I. D. Kim, *ACS Nano* **2023**, *17*, 23347.
[100] H. Zhao, B. Song, H. Li, X. Li, C. Ce, Q. Wu, J. Chen, Z. Wang, G. Yan, J. Fang, *Small* **2024**, *21*, 2407700.
[101] I. Jang, S. Lee, D. Kim, V. K. Paidi, S. Lee, N. D. Kim, J. Y. Jung, K. S. Lee, H. K. Lim, P. Kim, S. J. Yoo, *Adv. Mater.* **2024**, *36*, 2403273.
[102] S. Y. Ha, S. Kim, *J. Electroanal. Chem.* **1999**, *468*, 131;
[103] R. Chen, H. Li, D. Chu, G. Wang, *J. Phys. Chem. C* **2009**, *113*, 20689.
[104] X. Cui, S. Yang, X. Yan, J. Leng, S. Shuang, P. M. Ajayan, Z. Zhang, *Adv. Funct. Mater.* **2016**, *26*, 5708.
[105] Y. Lin, Y. Wang, Y. Xu, H. Liu, X. Liu, L. Shan, C. Wu, L. Yang, L. Song, *Adv. Funct. Mater.* **2024**, *35*, 2417486.
[106] C. Zhang, N. Li, Y. Liu, T. Zhang, R. Zhang, Z. Zhao, *Small* **2024**, *21*, 2407463.

Boran Zhou is currently studying in the Department of Chemistry of Capital Normal University, studying for a Master's degree. Her research interests focus on electrocatalytic applications of single-atom catalysts.

Kaiyuan Liu (Ph.D. candidate, Beijing Institute of Technology) researches on pulsed discharge synthesis of single-atom/cluster catalysts. He graduated from the Beijing Institute of Technology with a B.Eng. (2018) and a M.Eng. (2021). He has published 18 papers, including 6 SCI papers in internationally renowned academic journals as the first author.

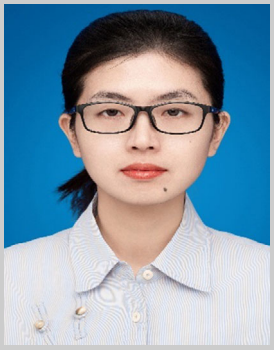

Yan Gao obtained her Ph.D. from the School of Chemistry and Chemical Engineering at the Beijing Institute of Technology in 2019. Her research interests encompass the precise construction of nano and single-atom catalysts and their application in energy catalysis. She has published more than 10 SCI papers in internationally renowned academic journals, either as the first author or corresponding author. These publications include prestigious journals such as Nano. Res., Chem. Commun., Atoms. Environ., J Mater. Chem. A.

Xin Gao is an associate professor at the School of Mechatronical Engineering, Beijing Institute of Technology. He earned his B.Eng. in mechanical engineering from Beijing University of Chemical Technology (2011) and a Ph.D. in engineering mechanics from the Beijing Institute of Technology (2018). He pursued postdoctoral research on pulsed discharge applications at Kumamoto University (2018–2020). He joined in Beijing Institute of Technology as an assistant professor in 2020. His work focuses on shockwave physical and chemical effects for nano-material synthesis, including nanomaterial fabrication by pulsed discharge or shock synthesis.

Zhengbo Chen, associate professor, Department of Chemistry, Capital Normal University. His research fields include recognition and detection of multiple targets by nanoenzyme optical array sensors; single colorimetric, electrochemical, and fluorescence sensitive sensing of targets by nanomaterial biosensors; medical applications of nanoenzymes in antibiotics and tumors; and applications of monoatomic catalysts in electrocatalysis.

Wenxing Chen obtained his B.S. degree from Beihang University in 2011. He subsequently earned his Ph.D. from the National Synchrotron Radiation Laboratory at the University of Science and Technology of China in 2015. In 2016, he joined Professor Yadong Li's group at the Department of Chemistry, Tsinghua University, as a postdoctoral researcher. Since 2018, he has been affiliated with the School of Materials Science and Engineering at Beijing Institute of Technology. His current research focuses on the rational design and synthesis of atomically dispersed metallic catalysts, along with their advanced characterization using synchrotron radiation techniques such as XANES and EXAFS.

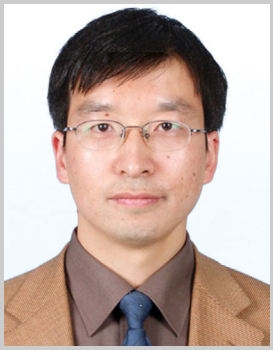

Pengwan Chen is a full professor at Beijing Institute of Technology, and the Dean of the School of Materials Science and Engineering at Beijing Institute of Technology. His research orientation focused on synthesis of advanced materials using dynamic high pressure, dynamic processing of materials, deformation and failure of materials. He published over 200 SCI papers, including papers published in Nater. Commun., Advan. Funct. Mater., Appl. Phys. Lett., he also has been granted over 60 authorized patents.